**Carbon Nanotube Arrays: Synthesis, Properties and Applications**

Suman Neupane, W.Z. Li

Department of Physics, Florida International University, Miami, FL 33199

## 1. Introduction

Carbon nanotubes (CNTs) have become one of the most interesting allotropes of carbon since the discovery of multi-walled carbon nanotubes (MWNTs) by Iijima [1] in 1991. It took almost two more years until Iijima et al. [2] and Bethune et al. [3] synthesized simultaneously single-walled carbon nanotubes (SWNTs). Ever since, steady progress has been made to successfully synthesize vertically and horizontally aligned arrays of CNTs over a wide range of substrates by employing different techniques. CNTs have shown promising mechanical, electrical, optical and thermal properties rendering their applications in new structural and functional materials, electrical circuitry, energy storage, drug delivery and many other devices of the future generation.

Several methods have been developed to synthesize CNTs with high purity and controllable diameter and length at desirable location over a wide variety of substrates. Among the available synthesis methods, arc discharge [1], laser ablation [4], chemical vapor deposition (CVD) [5], diffusion flame deposition [6] and electrochemical synthesis [7] are commonly used techniques for the synthesis of CNTs. A scalable device application requires the ability of control over the alignment of CNTs. In this paper, we will review the current state-of-the-art synthesis, properties, characterization and applications of CNTs. In section 2, the CNT synthesis techniques will be discussed. Then section 3 will focus on the fabrication mechanism of CNT arrays (CNTAs), section 4 on

mechanical properties, section 5 on thermal properties and section 6 on electrical properties. In section 7, we will discuss some applications of CNTs and finally, this review concludes with a summary.

## 2. Carbon Nanotube Synthesis

### 2.1 Arc discharge

MWNTs were synthesized originally by Iijima [1] using the arc discharge method (Fig. 1(a) ). A high direct current (d. c.), typically of the order of 200 A, between two graphite electrodes at a potential difference of 20 V, was maintained inside a chamber filled with Ar gas at 100 torr resulting in MWNTs. These MWNTs had diameters between 4 - 30 nm and up to 1 μm in length with the separation of 0.34 nm between the graphitic planes (Fig. 1(b)). Introduction of 10 torr methane and 40 torr Ar with Fe as catalyst was conducive for the growth of SWNTs [2] with diameters ranging between 0.7- 1.6 nm and length as long as 700 nm (Fig. 1 (c)). Large scale synthesis of MWNTs with 75% conversion of graphite was achieved by Ebbesen et al. [8] using helium gas at pressure of 500 torr and electrical potential difference of 18 V between the electrodes for optimum results. Journet et al. [9] synthesized SWNTs on a large scale using a mixture of metallic catalysts in a He environment at 500 torr using arc discharge.

### 2.2 Laser ablation

Guo et al. [4] pioneered the production of MWNTs by using Nd:YAG laser pulses over a graphite target heated to 1200ºC inside a 50 cm long, 2.5 cm diameter quartz tube (Fig. 2). The region inside the tube was maintained at 500 torr by flowing the Ar gas at a linear flow rate of 0.2 – 2 cm/s. Nanotubes are collected on the copper rod cooled by

circulating water. The as-synthesized MWNTs consisted of 4-24 layers of graphite and were 300 nm long. The quality of the MWNTs declined as the oven temperature was reduced from 1200 ºC to 900 ºC until no nanotubes were formed at 200 ºC. Thess et al. [10] optimized the process by adding transition metal catalysts to the graphite target to produce metallic SWNTs with yield greater than 70%. These uniform SWNTs (Fig. 3) self –organized into ropes like bundles of 5 – 20 nm in diameter and several micrometers in length. These bundles exhibit metallic transport property with resistivity less than $10^{-4}$ Ω·cm at 300 K.

**2.3 Electrochemical synthesis**

Matveev and co-workers [7] synthesized MWNTs from a $C_2H_2$ solution in liquid $NH_3$ below room temperature at 233K without a metal catalyst. Laboratory prepared pure dry $C_2H_2$ was mixed with liquid $NH_3$ formed by cooling gaseous ammonia to get 15 – 20 mol. % $C_2H_2$ solution and poured in a glass vessel for electrolysis. A d.c. voltage of 150 V was applied for 5–10 h between n-type silicon (100) electrodes of dimensions 5 mm×5 mm×0.3 mm. After electrolysis, the immersed part of the cathode was covered by a light-gray porous layer with average thickness of 1–2 μm. The MWNTs consisted of 10-20 graphite layers and had an average diameter of 15 nm with a high aspect ratio greater than 1000. The atomic hydrogen generated on the cathode initiated chain radical reactions and liquid $NH_3$ promoted these reactions by stabilization of radicals, this process facilitates the growth of CNTs.

**2.4 Diffusion flame synthesis**

Wal et al. [6] and Yuan et al. [11, 12] have demonstrated the synthesis of SWNTs via a less known simple laboratory-scale diffusion flame at temperatures between 1200ºC -1500ºC. A combined flow of $CH_4$ and air was used to ensure the production of stable, visible, laminar flame of height 65 mm at normal atmospheric pressure. CNTs were deposited on a stainless steel grid held in the flame and supported by a 0.4 mm wire of an alloy of Ni-Cr-Fe for 10-30 min. The spaghetti- and bamboo-shaped CNTs produced were between 20-60 nm in diameter.

**2.5 Chemical vapor deposition**

Yacaman et al. [5] used catalytic decomposition of carbon containing gas over a metal surface to grow carbon filaments and CNTs at relatively lower temperatures than that in arc-discharge and laser ablation methods. Fe catalyst uploaded on graphite substrate was obtained by impregnating the substrate in a 40 vol % ethanol / 60 vol % water solution of iron (III) oxalate. The iron oxalate impregnated graphite substrate was then reduced in the mixture of $N_2$ and $H_2$ at 350ºC to convert the iron oxalate into metallic Fe catalyst particles and then CNTs were grown by the introduction of a mixture of $N_2$ and carbon source gas $C_2H_2$ at 700ºC for several hours at standard atmospheric pressure. The as-grown CNTs measured 5 -20 nm in diameter and 50 μm in length. The diameter distribution and length could be controlled by the variation of concentration of catalysts and the time of reaction for the synthesis of CNTs. Transition metals Ni [13], Co [14] and Fe [15] catalysts were used successfully to synthesize CNTs using carbon precursors like $CH_4$, $C_2H_2$, $C_2H_4$ and others. Li et al. [16] used a CVD technique to grow aligned CNTs perpendicular to a silica substrate in a large scale. Mesoporous silica containing iron nanoparticles were prepared by a sol-gel process from tetraethoxysilane

hydrolysis in an iron nitrate aqueous solution. $C_2H_2$, diluted by $N_2$, was used as the carbon precursor gas to grow CNTs on Fe catalyst nanoparticles formed after the reduction of the iron oxide nanoparticles. Scanning electron microscopy (SEM) images revealed the vertically aligned CNTs having diameters ~ 30 nm with spacing of ~ 100 nm (Fig 4). The length of individual CNTs in the films is approximately 50 μm. The high resolution TEM images show the presence of around 40 concentric shells of graphite in an individual CNT with a spacing of ~ 0.34 nm between the layers. The array consists of pure CNTs without catalyst particles or amorphous carbon.

Kong et al. [17] synthesized horizontally oriented SWNTs over a patterned Si substrate using CVD. A thin film of 0.25 μm polymethylmethacrylate (PMMA) was deposited on the Si substrate using spin coating at 4000 rpm. Square holes were fabricated on the PMMA film by an electron beam lithography. The exposed PMMA was removed by using organic solvents. Different solutions containing catalyst of Fe, Mo or Al was deposited on the patterned PMMA substrate. Finally, the PMMA film was removed by heating and subsequently treating with 1, 2-dichloroethane. The catalyst islands formed squares of 3 or 5 μm spaced at 10 μm on the Si substrate (Fig. 5).The SWNTs were synthesized using $CH_4$ as the carbon precursor gas at 1000ºC. The as-synthesized SWNTs were 1- 3 nm in diameter and ran several micrometers in length (Fig. 5).

## 3. Carbon Nanotube Arrays

The unique stability, and structural, electrical, and mechanical properties render the possibility of using CNTs in a number of applications such as advanced scanning probes [18], nanoelectronic devices [8, 9], and electron field emission sources [19, 20].

However, for electronic applications, it is desirable to have high-quality CNTs in a controlled pattern in order to avoid post-growth treatments which generally give rise to defects and impurities. With this view point, CNT arrays (CNTAs) have been fabricated directly over silicon [21], quartz [22], steel [23], nickel [24], titanium [25], copper [26], platinum [27] , sapphire [28], silicon carbide [29], and others. The process of production of CNTAs starts with pre-positioning the catalyst on the substrates. The control of CNT production has been achieved by the deposition of catalyst in a predetermined pattern using pulsed laser deposition (PLD) [30], anodic aluminum oxide (AAO) templates [21, 31], reverse micelle method [32], photolithography [33], electrochemical etching [34], sputtering [35, 36], nanosphere lithography [37], sol-gel method [38], and other methods. CNTA synthesis has been carried out by CVD and modified forms of CVD like d.c. plasma enhanced chemical vapor deposition (PECVD) [22], microwave PECVD [39] and others. D.C. bias sputtering [40], electrophoretic deposition [41], screen printing [42] etc have also been used to form well aligned CNTAs. Horizontal and vertical alignment of CNTs has been successfully achieved using the aforementioned methods.

### 3.1 CNTA synthesis using patterned catalyst arrays

The most efficient method of forming well aligned CNTA is to deposit catalysts in a predetermined pattern to grow CNTs selectively. Commonly used methods for catalyst patterning are described below.

#### 3.1.1 Pulsed laser deposition

Pulsed laser deposition (PLD) utilizes laser signals of predetermined pulse width of several tens of nanoseconds to strike on a rotating target material. Saurakhiya et al. [30] used a 248 nm KrF laser with a pulse width of 23 ns and a repetition rate of 10 Hz on a

rotating iron target inside a vacuum chamber with base pressure of ~ $10^{-6}$ torr (Fig. (6)). The left panel shows the schematic of PLD. The center and right panels show the SEM images of the square or hexagonal arrays of aligned CNTs synthesized on the square or hexagon shaped catalyst arrays. The square or hexagonal pattern of catalyst on silicon and quartz substrates was obtained by utilizing TEM copper grids as masks during the PLD catalyst deposition. An aluminum sheet was used to hold and press the Cu grids to keep them as close as possible to the substrates. The thickness of the Fe film was controlled by varying the deposition time, laser power, and the distance between the target and substrate. Vertically aligned CNTs were produced by PECVD using $C_2H_2$ and $H_2$ at 700ºC.

### 3.1.2 Anodic aluminum oxide (AAO) templates

Anodic aluminum oxide (AAO) templates with ordered nanohole arrays have been made by a two-step anodization of alumium (Al) [21, 31]. During a typical double anodization process, a clean Al sheet is first anodized at 40 V in a 0.3 M oxalic acid for 5–6 hrs at room temperature. Then the disorderly anodic oxide layer formed during the process is removed in a mixture of phosphoric acid and chromic acid. The anodization process is repeated under the same conditions for 3–4 hrs which results in the formation of highly ordered porous AAO templates. The pores have diameters of ~ 50 nm and are ~ 100 nm apart. Figure 7 shows the SEM images of top views and cross-sectional views of typical arrays of AAO nanopores formed using double anodization process.

### 3.1.3 Reverse micelle method

In a reverse micelle method, metal salts are reduced to metal nanoparticles in a nanoscale water pool inside a glove box filled with nitrogen gas to prevent oxidation.

Ago et al. [32] used didodecyldimethylammonium bromide (DDAB) as the cationic surfactant and sodium borohydride ( $NaBH_4$) as a reducing agent to obtain catalyst cobalt particles from a cobalt chloride ($CoCl_2.6H_2O$) solution. The surfactants help to stabilize the nanoparticles. DDAB was dissolved in toluene with a 10 wt % concentration, followed by dissolving $CoCl_2.6H_2O$ to a concentration of 0.005 M. With the addition of 5 M $NaBH_4$ aqueous solution and continuous stirring, the solution turned from light blue to black due to the formation of colloidal dispersion of Co nanoparticles. The as-prepared Co nanoparticles were purified further by repeating centrifugation and redispersion in toluene and acetone. The colloidal dispersion of the Co nanoparticles was finally cast on Si substrate and dried at room temperature. The TEM image showed that the Co nanoparticles with average diameter 4 nm were well separated due to the presence of surfactants that covered the surface of the nanoparticles. The size of the nanoparticles could be altered by tuning the concentration of $NaBH_4$ solution. Vertically aligned CNTs were synthesized using CVD.

### 3.1.4 Photolithography

Photolithography is the mechanism of transferring a geometrical pattern onto a substrate using light. The photo-sensitive material called resist will form desired patterns upon light exposure through photomasks. Catalysts are preferentially deposited by a suitable approach and the resist is generally removed by chemical etching (Fig. 8). The process of photolithography starts with the application of a thin and uniform layer of photoresist to the surface of the wafer by spin coating at the speed of 1000-5000 rpm for a period of 30-60 s. The photo resist-coated wafer is then prebaked at the temperature of 100 °C to remove excess photoresist solvent for 30-60 s. The prebaking is followed by

exposure of the photoresist to ultraviolet (UV) light through a suitably designed mask. A positive resist becomes soluble to the developer solution upon exposure to the UV while a negative resist becomes insoluble upon similar UV treatment. The UV exposed substrate is immersed in a developer solution to remove the photoresist and obtain the desired pattern. The resulting wafer is then hard baked at around 200 °C to solidify the photoresist. A suitable layer of the catalyst is then deposited by e-beam evaporation, sputtering or other methods. Finally, the photoresist is removed by wet etching in chemical solutions, oxygen plasma etching or other methods. Wei et al. [33] synthesized well aligned CNTs by CVD on patterned catalyst nanoparticles formed by using photolithography . The density of the CNTAs can be controlled by the pattern geometry on the masks used in the photolithography process.

### 3.1.5 Electrochemical etching

Xu et al. [34] have synthesized CNTA using electrochemical etching and selectively depositing catalysts in a pre-defined pattern. The micro-, meso- and macro-porous Si substrates were produced in an electrochemical etching cell containing an aqueous HF solution. Platinum wire was used as a cathode and the crystalline Si wafer acted as an anode. Thin Al films were evaporated on the back of the wafers to ensure good ohmic contact before anodization. The electrolyte for the anodization was made using 48% HF and ethanol in a ratio of 1:1. A current density of 1–80 $mA/cm^2$ was maintained in darkness for 1–10 min depending on the desired thickness and porosity. Nickel catalyst was deposited on the pores by immersing the substrates in a nickel acetate solution for 24 hrs. Then the CVD method was adopted to synthesize CNTA by using $H_2$

and Ar as reducing gases and $C_2H_4$ as the carbon precursor at 880 °C on the patterned Ni nanodots on the Si substrate.

### 3.1.6 Sputtering

CNTAs have been synthesized using thin films of catalysts deposited by ion beam sputtering [36], d.c. magnetron sputtering [40], r.f. magnetron sputtering [43], and reactive sputtering [44]. The target material, which is usually a circular disc, is placed inside a high vacuum chamber at a certain distance from a substrate. Sputtering is usually carried out in an inert Ar atmosphere in the presence of a d.c. power supply or an r.f. generator. Wang et al. [35] have used d.c. magnetron sputtering to form 20 nm thin films of Ni on Si and then have synthesized well aligned CNTA using PECVD using the Ni thin film as catalyst. $C_2H_2$ was used as the carbon precursor gas to produce vertically aligned CNTs around 1 μm long in less than 5 minutes at ~ 550-600°C

### 3.1.7 Nanosphere lithography

Nanosphere lithography **(**NSL) is another powerful tool to form patterns of catalysts for well-controlled growth of CNTAs. The process starts with making Si wafers hydrophilic by treating them with an RCA solution which is a mixture of $NH_4OH$, $H_2O_2$ and water in the volume ratio 1:1:5. Then sub-micron sized polystyrene spheres (PS) dispersed in methanol is spin-coated onto Si substrate to obtain a monolayer of PS. The catalyst layer is deposited by e-beam evaporation or other methods followed by the removal of the PS layers through wet etching. The hexagonal patterns of catalyst obtained can be used to grow CNTAs by CVD and PECVD methods [37, 45, 46]

### 3.1.8 Sol-gel method

The Sol-gel method has been employed to form mesoporous silica containing Fe catalysts to grow CNTAs by CVD. Li et al. [14, 38] formed a mixture of tetraethoxysilane (TEOS) in ethyl alcohol and aqueous solution of iron nitrate by magnetic stirring for ~30 min. A few drops of concentrated hydrogen fluoride were then added to form a gel. The gel was dried for one week at 60°C to remove the excess water and other solvents, followed by calcination for 10 hours at 450°C at $10^{-2}$ torr. A uniform porous silica network was obtained with iron oxide nanoparticles embedded in the pores. The iron oxide nanoparticles were then reduced to Fe nanoparticles at 550°C in the continuous flow of $N_2$ and $H_2$ for 5 h. Acetylene ($C_2H_2$) was used as the carbon source for the CVD process of CNT synthesis to obtain vertically aligned arrays of CNTs. The well graphitized tubes as long as 50 μm were synthesized with the spacing of 100 nm between the tubes (Figure 4).

**3.2 CNTA synthesis by other methods**

Joselevich [47] has investigated the application of an electric field to produce aligned SWNTs. The SWNTs align in the direction of an electric field and perpendicular to the direction of gas flow by minimizing the Van der Waals interactions with the nearby surfaces. The electric field between the electrodes will induce a dipole in each growing SWNT. The electric field then exerts a torque on those induced dipoles forcing CNTs to grow parallel to the direction of the electric field. Zhang et al. [48] have used d.c. (0-200V) or an a.c. (30 MHz, 10V peak-to-peak) voltage between catalyst islands to produce aligned SWNTs on quartz by CVD. The optimum electric fields for the directed growth of suspended SWNTs were in the range of 0.5 V/μm. Absence of an electric field resulted in random CNTs.

Lee et al. [49] demonstrated the lateral alignment of CNTs as the result of applying magnetic field during the process of catalyst dispersion on silicon substrates. The growth direction of CNTs was found to be perpendicular to the direction of applied magnetic field. Kumar et al. [50] used a bacterium Magnetospirillium magnetotacticum, which synthesizes intracellular, linear, single domain magnetic nanoparticles through highly regulated biomineralization, to produce highly orientated MWNTs on silicon oxide substrates by CVD. A magnetic bar of strength 17 mT was used to investigate the effects of magnetic field on CNT growth. The average diameter of MWNTs was 13 ± 3.6 nm and the samples grown on the magnetotactic bacteria show the preferential direction of growth along the magnetic field. This suggests the possibility of synthesis of dimensionally controlled and spatially oriented CNTs by exploiting various magnetotactic bacteria as catalyst carriers with an applied magnetic field.

**3.3 Horizontal arrays of CNTs**

Horizontal arrays of CNTs also have shown a lot of potential for device fabrication and have been successfully grown by different groups. Huang et al. [51-53] have grown millimeter long and horizontally aligned SWNTs on silicon substrates by the fast heating CVD process (Fig 9(a)). A slow heating process resulted in random alignment of CNTs as compared to good horizontal alignment obtained by rapid heating. A two-dimensional network of SWNTs has been directly grown on the substrates by a two-step growth process (Fig 9(b)) by altering the direction of flow of gases in subsequent stages. The well defined crossed network structure of SWNTs on a large scale enables the fabrication of multiterminal devices and complex circuits necessary for various applications.

## 4. Mechanical Properties

CNTs exhibit tremendous strength as the consequence of carbon-carbon bonding which is considered to be the strongest bonding in nature. This property along with the low density and fibril shape lead to the exploration of the viability of CNTs as a reinforcement material in composites. Theoretical calculations by Sanchez-Portal et al. [54] predicted the exceptionally high Young's modulus of SWNTs and MWNTs. The Young's modulus depends upon the radius of the CNTs considered. Treacy et al. [55] measured the Young's modulus of individual CNTs by measuring the amplitude of their intrinsic thermal vibrations inside a transmission electron microscope. The measurement of 11 CNTs ranging from 0.66 – 5.81 μm in length yielded an average Young's modulus of 1.8 TPa with higher modulus for thinner CNTs.

Wong et al. [56] employed an atomic force microscope (AFM) to measure the mechanical properties of the CNTs and found the Young's modulus of MWNTs was about 1.3 TPa. Gao et al. [57] and Hernandez et al. [58] estimated theoretically the Young's modulus of individual SWNTs were at the range of ~ 0.4-0.6 TPa. Experimentally, Yu et al.[59] obtained an average value of 1 TPa and Zhu et al. [60] obtained an average value of ~100GPa for strands of SWNTs of diameter ~5-20 μm. These values are dependent on the crystallinity of the materials and number of defects introduced during the process of synthesis and measurement. Arrays of CNTs exhibit a high adhesive force of the magnitude of 100 $Ncm^{-2}$ and much stronger shear adhesion force than normal adhesion force [61]. Based on the theoretical and experimental results, CNTs are found to exhibit large Young's Modulus of elasticity making them a viable supplement for rigid materials.

## 5. Thermal Properties

The specific heat capacities and thermal conductivities of carbon nanotube are due to contributions of phonons. The behavior of phonons at different temperatures completely describe the thermal transport properties of CNTs. Figure (10) shows the specific heat capacity of SWNTs which exhibits the linear dependence on temperature from 300 K to 1K [62, 63] while exhibiting ~ $T^{0.62}$ dependence below 1 K [64]. The linear temperature dependence is due to the linear k-vector dependence of the frequency of the longitudinal and twist acoustic phonons. The specific behavior of the specific heat below 1 K can be attributed to the transverse acoustic phonons with quadratic k dependence [65]. The results indicate that inter-wall coupling in MWNTs is rather weak compared with its parent form, graphite, so that one can treat a MWNT as a few decoupled two-dimensional single wall tubules [63]. Figure (11) shows the expansion of Fig. (10) in the lower temperature region. The solid dots represent the initial run and open circles were recorded during rapid cooling after first warming to 77 K. The open triangles are for the measurements of CNTs kept overnight in the helium environment at the temperature of 4 K. There is a slight deviation from the original behavior of specific heat capacity of SWNTs due to He adsorption.

The thermal conductivity of MWNTs is roughly linear above ~120K and becomes quadratic at lower temperatures, Figure 12 [63]. Kim et al. [66] measured thermal conductivity using a suspended microdevice (Fig 13). The observed thermal conductivity is more than 3000W/K·m at room temperature, which is 2 orders of magnitude higher than the estimation from macroscopic mat samples [63]. The

temperature dependence of the thermal conductivity of nanotubes exhibits a peak at 320 K due to the onset of Umklapp phonon scattering (Fig 14). Berber et al. [67] theoretically determined an unusually high value of 6600 W/K·m for an isolated (10, 10) nanotube at room temperature, comparable to the thermal conductivity of a hypothetical isolated graphene monolayer or diamond by combining equilibrium and non-equilibrium molecular dynamics simulations. These high values are associated with the large phonon mean free paths in the CNTs, graphene monolayer and diamond systems while substantially lower values are predicted and observed for the basal plane of bulk graphite. The numerical data indicate that, in the presence of interlayer coupling, the thermal conductivity of the CNTs is reduced significantly to fall into the experimentally observed value range.

Shaikh et al. [68] have demonstrated the high thermal conductivity (8.3082 W/m·K) of CNT film consisting of vertically aligned CNT arrays prepared using CVD on a glass substrate in comparison to using CNT composite film (1.2 W/m·K) by Huang et al. [69] . This proves the superiority of CNTAs over films for thermal interface material. Owing to the superior thermal conductivity, Xu et al. [70] have demonstrated the possibility of using CNTAs for integrated circuit cooling.

## 6. Electrical properties

CNTs are perfect one-dimensional conductors and exhibit interesting phenomena such as single-electron charging, resonant tunneling through discrete energy levels and proximity-induced superconductivity. Langer et al. [71] reported on the electrical resistance of a MWNT bundle from room temperature down to 0.3 K under magnetic

fields of up to 14 T. The nanotubes exhibited semi-metallic behavior analogous to rolled graphene sheets with a similar band structure. A magnetic field applied perpendicular to the sample axis decreases the resistance. Langer et al. [72] later reported on the electrical resistance measurements of an individual CNT down to a temperature of 20 mK. The conductance exhibits logarithmic temperature dependence and saturates at low temperatures. A magnetic field applied perpendicular to the tube axis increases the conductance and produces aperiodic fluctuations.

Bockrath et al. [73] measured the electrical properties of bundles of SWNTs. A gap due to suppressed conductance at low bias is observed in the current-voltage curves at low temperatures (Fig 15). Further, several prominent peaks are observed in the conductance as a function of a gate voltage which can be explained considering Coulomb blockade transport in quantum wires and dots considering CNTs as extended quantum dots. Theoretical calculations predict the metallic conductivity of individual SWNTs [74].

Tans et al. [75] measured the electrical characteristics of individual SWNTs at different gate voltages. Figure 16 shows the I-V curves at gate voltage of 88.2 mV for trace A, 104.1 mV for trace B and 120.0 mV for trace C. The inset shows similar I-V curves with gate voltage ranging from 50mV (bottom) to 136 mV (top). The I-V curves showed a clear gap around zero bias voltage. For higher voltages, the current increases in steps. The gaps were suppressed for certain gate voltages and have the maximum value corresponding to zero bias voltage. This variation of the gap with gate voltage around zero bias voltage implies Coulomb charging of the tube. Zhu et al. [76] used a lift-off process to pattern catalysts and synthesize vertical CNT arrays using CVD. Two-probe electrical measurements of the CNT arrays indicate a resistivity of 0.01 Ω·cm compared

to $8 \times 10^{-4}$ Ω·cm and $12 \times 10^{-4}$ Ω·cm of individual SWNTs, and the capacitance of the nanotube bundle was ~ 2.55 pF as the voltage was scanned from -1 V to 1 V, suggesting possible use of these CNTs as interconnect materials [76] .

CNTs are a good source of electrons through the process of field emission. The experimental set up to measure the field emission property is shown in Fig. (17). CNTs are used as cathodes and a high electric field of the order of ~2V/μm is created between a metal anode and the CNT cathode to measure electron emission in a low vacuum of about $\sim 10^{-7}$ torr. de Heer et al. [77] determined the emission characteristics of films of oriented nanotubes [78] and as grown CNTAs [20, 34, 79]. Yuning et al. [80] demonstrated well agreement between the experimental and theoretical values of emission behavior of CNTAs. The total emission current depends upon the CNTs radius (r), height (h) and spacing (d). The optimum space between two neighboring CNTs is about 75r and the height should be larger than 2.6d to obtain a large average current density. Hajra et al.[81] have observed the dramatic enhancement in the emission current density by a factor >106 with the onset field as low as 0.16 V/μm by using the plasma-sharpened tips of nanotubes containing only a few tubes at the apex of the structure (Fig. 18 ). Saturation in the emission current density is proposed due to the significant change in the tunneling barrier for a nanosized tip in a very high local electric field. Saurakhiya et al.[30] observed similar decrease in the threshold voltage of the as-grown CNTAs by laser pruning. In laser pruning process, the as-grown CNTs were irradiated by a He-Ne laser light with a wavelength of 632.8 nm and a power of 30 mW. Laser pruning resulted in the decrease of length of the CNTs by around 2 μm and better alignment of the CNTs. Zhao et al. [82] demonstrated that arrays of CNTs with large wall numbers exhibited

lower threshold voltages. To achieve a lower threshold voltage, an array of small diameter nanotubes with large intertube spacing (2 times the height) would be ideal. However, this situation was not easily achievable, as nanotube diameter and intertube spacing were in competition. In this case, the intertube spacing appeared dominant because the threshold voltage decreased despite increasing diameter. This means that intertube screening effects, that reduce the local electric field, are more dominant than the diameter on the resulting threshold voltage. Suh [31]et al. studied the field-screening effect of highly ordered CNTAs and concluded that the field emission was optimal when the tube height was similar to the intertube distance in agreement with the predictions by Nilsson et al. [83]. Charlier et al. [84] demonstrated that boron doped CNTs exhibited better field emission with lower threshold voltage than pristine CNTs. In general, the straight line observed in the Fowler-Nordheim plot is the evidence of field-emission (Fig. 19).

## 7. Applications of CNTs and CNTAs

### 7.1 Hydrogen storage

CNTs have high potential for hydrogen storage as the gas can effectively condense to a high density inside narrow SWNTs. Dillon and coworkers [85] compared the hydrogen storage capacity of carbon soot containing only about a 0.1 to 0.2 weight percentage of SWNTs to that of the activated carbon (AC) at 133 K. The SWNTs with diameter of 1.2nm were synthesized in an electric arc discharge process. The adsorption of hydrogen on the SWNTs was probed with temperature programmed desorption (TPD) spectroscopy in an ultrahigh vacuum chamber inside a liquid nitrogen cryostat. $H_2$

desorbs from SWNTs and activated carbons within the same temperature range but with different intensities. The signal from SWNTs is ~ 10 times greater than the signal from AC with the gravimetric storage density in SWNT ranging from ~5% to 10 wt % (Fig 20).

Liu [86] et al. studied the hydrogen storage of SWNTs with mean diameter 1.85 nm, and purity in the range of 50 to 60 wt % at room temperature. Fig. 21 shows the uptake of $H_2$ for three samples. Sample 1 was used as-synthesized; sample 2 was soaked in 37% HCl acid for 48 hrs to partly eliminate the residual catalysts, rinsed with deionized water and dried at 423K; sample 3 was heated in vacuum at 773K for two hrs after receiving the same treatment as sample 2. The heat treatment is to evaporate the organic compounds and functional groups formed in SWNTs during the synthesis procedure. A hydrogen storage capacity of 4.2 wt % was achieved at the pressure of 10 MPa. Furthermore, about 78.3% of the adsorbed hydrogen (3.3 wt %) could be released under ambient pressure at room temperature. Ye et al. [87] demonstrated the adsorption of $H_2$ exceeding 8 wt % on highly purified crystalline ropes of SWNTs at temperature of 80K and pressure of ~100Pa.

Zhu et al. [88] measured the $H_2$ absorption of well aligned and randomly ordered MWNTs produced by catalytic pyrolysis on quartz substrate at 290 K and pressure between 3-10 MPa. Figure 22 shows that the bundles of aligned MWNTs are better suitable for hydrogen adsorption as compared to randomly ordered MWNTs under similar conditions. This higher $H_2$ absorption capacity of 3.4 wt % of CNTA as compared to 0.5 wt% of the random-MWNTs can be attributed to the strong interaction between the hydrogen molecules in the interstitial channels between the CNTs and the inter-layers of some cap-opened CNTs. Wang et al. [89] have performed classical grand canonical

Monte Carlo simulations to calculate the absorption of hydrogen in tube arrays at 77K and 298K. The tube lattice spacing has been varied to study the optimum hydrogen uptake using triangular and square lattices. The strength of the solid-fluid interaction potential has been increased in order to identify a combination of potential and geometry that will meet the Department of Energy (DOE) targets of 6.5 wt % for hydrogen storage for fuel cell vehicles. The DOE target values could not be reached even by tripling the fluid-wall potential at ambient temperatures. However, it was possible to achieve the DOE targets at a temperature of 77 K, if the strength of the interaction potential was increased by about a factor of 2 and the lattice spacing of the tubes was optimized.

Misra et al. [90] used electrically conducting surfaces of CNTAs as cathodes for $H_2$ generation and absorption by electrolyzing water. Figure 23 shows the experimental setup used for the electrolytic measurements on the CNTAs. An electrochemical cell was assembled by inserting a metal tip connected to a power supply with the deionized water bubble on top of CNTA acting as the cathode. D.C. measurements were performed using a Cascade, M150 probe station, attached to a Keithley-2635 source inside a vacuum chamber. An application of external voltage (-10V) between the electrodes resulted in collection of hydrogen gas near the surface of the CNTA due to the electrochemical deposition of water. The amount of $H_2$ measured ($2.2 \pm 0.35 \times 10^{-5}$ gm) is less than the theoretical amount of hydrogen generated ($2.6 \times 10^{-4}$ gm) from flowing current over a period of 1 hr supporting the possibility of use of aligned CNTs as the $H_2$ storage materials.

**7.2 CNTs as Sensors**

CNTs can be used as chemical or biological sensors by exploiting their variation in optical, electrical, and electrochemical properties. For example, upon exposure to the gaseous molecules like $NH_3$, $NO_2$, $H_2O_2$ etc or biological species such as enzymes, CNTs exhibit a dramatic increase or decrease in resistance. Sensitivity and recovery time are two key components for the sustainable use of CNTs in detection of foreign elements.

Kong et al. [91] studied the electric response of semiconducting SWNTs before and after the introduction of $NH_3$ and $NO_2$. The I-$V_g$ curve shifted by -4 V or +4V when $NH_3$ or $NO_2$ was introduced into the chamber, respectively (Figure 24).These shifts can be explained by the depletion or enhancement of hole carriers brought about by the introduction of the respective gases [91]. Qi et al. [92] used arrays of electrical devices each comprised of multiple SWNT sensors with 100% yield for detecting gas molecules. Polymer functionalization was used to impart high sensitivity and selectivity to the sensors to fabricate n-type nanotube devices capable of detecting $NO_2$ at less than 1 ppb (parts-per-billion) concentrations while being insensitive to $NH_3$. CNTAs have been effectively used to detect glucose [27, 93] , $H_2O_2$ [93], DNA [94], protein [95], and others by tracking their electrical or optical response before and after the introduction of particular species.

**7.3 CNTs for battery and supercapacitor applications**

CNTs can find their applications as electrode materials for highly efficient batteries due to their high electrochemical stability, large surface area, and unique electrical and electronic properties. SWNTs exhibits higher capacity of Lithium (Li) intercalation than graphite and disordered carbon. Theoretical calculations [96] predicted the possibility of almost complete charge transfer between Li and SWNTs with relatively small

deformation in the structure. Both the interstitial sites and inner side of the tubes are energetically favorable sites for Li intercalation. Theoretical calculations predict the possibility of one Li atom intercalation for every two carbon atoms. Cyclic voltammograms [97] confirm that the reversible intercalation of $Li^+$ and presence of Fe, Pt, or Ru nanoparticles within the tube will double the intercalation capacity.

Figure 25 shows the cyclic efficiency of graphite as a function of added weight percent of CNTs. The efficiency of graphitic anodes increased continuously until the composition of 10 wt % CNTs which resulted in an efficiency of almost 100% up to 50 cycles [98]. Wu et al. [99] demonstrated high Li ion storage capacity at 700 $mAhg^{-1}$ by CNTs. Gao et al. [100] improved the storage capacity from 400 $mAhg^{-1}$ for as-prepared SWNTs to 700 $mAhg^{-1}$ after removing impurities and 1000 $mAhg^{-1}$ by ball-milling the SWNTs.

The super-capacitance property of CNTs has also been extensively studied because they are able to store and deliver energy rapidly and efficiently for a long life cycle via a simple charge separation process. Ma et al. [101] were able to construct electrochemical capacitors based on CNT electrodes with specific capacitances of about 25 F $cm^{-3}$ with 38 wt. % sulphuric acid as the electrolyte. An et al. [102] reported a maximum specific capacitance of 180 F/g and a measured power density of 20 kW/ kg at energy densities in the range of 7 to 6.5 Wh/kg by using SWNTs as electrode material in supercapacitors. Similar measurements also reported the specific capacity of 102 F/g for the electrodes using MWNTs [103].

**7.4 CNTs for photovoltaic device**

Ago et al. [104] fabricated a photovoltaic device (Fig 26) using MWNTs as an electrode to collect holes and obtain an efficiency double that of the standard device with an indium-tin oxide (ITO) electrode. The visible light is shown through a semi-transparent Al electrode and made to pass through polyphenylene vinylene (PPV) of thickness 210 nm and MWNT film of thickness 140nm in the photovoltaic device. The I-V characteristics (Fig 27) expressed a clear diode rectification. Upon illumination of the device by light of wavelength 485 nm and intensity 37 $\mu W/cm^2$, a photocurrent was observed with open-circuit voltage of 0.90 V and short-circuit current of 0.56 $\mu A/cm^2$. The external quantum efficiency of MWNT/PPA/Al was typically 1.5 to 2 times greater than the standard ITO device. The higher efficiency could be attributed to the complex interpenetrating network of PPV chains with the MWNT film and the relatively high work function of the MWNT film. Lagemaat et al. [105] have also reported similar successful replacement of $In_2O_3$ : Sn by CNTs in an organic solar cell.

## Conclusions

In this paper, the synthesis techniques and the mechanical, electrical, and thermal properties of the CNTs, especially the CNTAs, have been reviewed. We have also discussed some promising applications of CNTs and CNTAs in hydrogen storage, biological and chemical sensors, lithium batteries, and photovoltaic devices. To explore the applications of CNTAs, CNT arrays with controllable nanotube diameter, density, spacing, and degree of defects are extremely important. In addition, for wide applications of the CNTAs, methods for synthesizing aligned CNTs at the conditions compatible with current fabrication techniques of nanodevices need to be developed.

**References:**


[1] S. Iijima, "Helical Microtubules of Graphitic Carbon," *Nature,* vol. 354, no. 6348, pp. 56-58, Nov 7, 1991.

[2] S. Iijima, and T. Ichihashi, "Single-Shell Carbon Nanotubes of 1-Nm Diameter," *Nature,* vol. 363, no. 6430, pp. 603-605, Jun 17, 1993.

[3] D. S. Bethune, C. H. Kiang, M. S. Devries *et al.*, "Cobalt-Catalyzed Growth of Carbon Nanotubes with Single-Atomic-Layerwalls," *Nature,* vol. 363, no. 6430, pp. 605-607, Jun 17, 1993.

[4] T. Guo, P. Nikolaev, A. G. Rinzler *et al.*, "Self-Assembly of Tubular Fullerenes," *Journal of Physical Chemistry,* vol. 99, no. 27, pp. 10694-10697, Jul 6, 1995.

[5] M. Joseyacaman, M. Mikiyoshida, L. Rendon *et al.*, "Catalytic Growth of Carbon Microtubules with Fullerene Structure," *Applied Physics Letters,* vol. 62, no. 2, pp. 202-204, Jan 11, 1993.

[6] R. L. Vander Wal, T. M. Ticich, and V. E. Curtis, "Diffusion flame synthesis of single-walled carbon nanotubes," *Chemical Physics Letters,* vol. 323, no. 3-4, pp. 217-223, Jun 16, 2000.

[7] A. T. Matveev, D. Golberg, V. P. Novikov *et al.*, "Synthesis of carbon nanotubes below room temperature," *Carbon,* vol. 39, no. 1, pp. 155-158, 2001.

[8] T. W. Ebbesen, and P. M. Ajayan, "Large-Scale Synthesis of Carbon Nanotubes," *Nature,* vol. 358, no. 6383, pp. 220-222, Jul 16, 1992.

[9] C. Journet, W. K. Maser, P. Bernier *et al.*, "Large-scale production of single-walled carbon nanotubes by the electric-arc technique," *Nature,* vol. 388, no. 6644, pp. 756-758, Aug 21, 1997.

[10] A. Thess, R. Lee, P. Nikolaev *et al.*, "Crystalline ropes of metallic carbon nanotubes," *Science,* vol. 273, no. 5274, pp. 483-487, Jul 26, 1996.

[11] L. M. Yuan, K. Saito, C. X. Pan *et al.*, "Nanotubes from methane flames," *Chemical Physics Letters,* vol. 340, no. 3-4, pp. 237-241, Jun 1, 2001.

[12] L. M. Yuan, K. Saito, W. C. Hu *et al.*, "Ethylene flame synthesis of well-aligned multi-walled carbon nanotubes," *Chemical Physics Letters,* vol. 346, no. 1-2, pp. 23-28, Sep 28, 2001.

[13] E. F. Kukovitsky, S. G. L'vov, N. A. Sainov *et al.*, "Correlation between metal catalyst particle size and carbon nanotube growth," *Chemical Physics Letters,* vol. 355, no. 5-6, pp. 497-503, Apr 8, 2002.

[14] J. Li, C. Papadopoulos, J. M. Xu *et al.*, "Highly-ordered carbon nanotube arrays for electronics applications," *Applied Physics Letters,* vol. 75, no. 3, pp. 367-369, Jul 19, 1999.

[15] A. M. Cassell, J. A. Raymakers, J. Kong *et al.*, "Large scale CVD synthesis of single-walled carbon nanotubes," *Journal of Physical Chemistry B,* vol. 103, no. 31, pp. 6484-6492, Aug 5, 1999.

[16] W. Z. Li, S. S. Xie, L. X. Qian *et al.*, "Large-scale synthesis of aligned carbon nanotubes," *Science,* vol. 274, no. 5293, pp. 1701-1703, Dec 6, 1996.

[17] J. Kong, H. T. Soh, A. M. Cassell *et al.*, "Synthesis of individual single-walled carbon nanotubes on patterned silicon wafers," *Nature,* vol. 395, no. 6705, pp. 878-881, Oct 29, 1998.

[18] H. Wang, J. Lin, C. H. A. Huan *et al.*, "Controlled synthesis of aligned carbon nanotube arrays on catalyst patterned silicon substrates by plasma-enhanced chemical vapor deposition," *Applied Surface Science,* vol. 181, no. 3-4, pp. 248-254, Sep 21, 2001.

[19] S. S. Fan, W. J. Liang, H. Y. Dang *et al.*, "Carbon nanotube arrays on silicon substrates and their possible application," *Physica E,* vol. 8, no. 2, pp. 179-183, Aug, 2000.

[20] Z. H. Yuan, H. Huang, H. Y. Dang *et al.*, "Field emission property of highly ordered monodispersed carbon nanotube arrays," *Applied Physics Letters,* vol. 78, no. 20, pp. 3127-3129, May 14, 2001.

[21] W. C. Hu, D. W. Gong, Z. Chen *et al.*, "Growth of well-aligned carbon nanotube arrays on silicon substrates using porous alumina film as a nanotemplate," *Applied Physics Letters,* vol. 79, no. 19, pp. 3083-3085, Nov 5, 2001.

[22] Z. F. Ren, Z. P. Huang, J. W. Xu *et al.*, "Synthesis of large arrays of well-aligned carbon nanotubes on glass," *Science,* vol. 282, no. 5391, pp. 1105-1107, Nov 6, 1998.

[23] C. Masarapu, and B. Q. Wei, "Direct growth of aligned multiwalled carbon nanotubes on treated stainless steel substrates," *Langmuir,* vol. 23, no. 17, pp. 9046-9049, Aug 14, 2007.

[24] Z. P. Huang, J. W. Wu, Z. F. Ren *et al.*, "Growth of highly oriented carbon nanotubes by plasma-enhanced hot filament chemical vapor deposition," *Applied Physics Letters,* vol. 73, no. 26, pp. 3845-3847, Dec 28, 1998.

[25] Y. Gao, J. Liu, M. Shi *et al.*, "Dense arrays of well-aligned carbon nanotubes completely filled with single crystalline titanium carbide wires on titanium substrates," *Applied Physics Letters,* vol. 74, no. 24, pp. 3642-3644, Jun 14, 1999.

[26] G. Li, S. Chakrabarti, M. Schulz *et al.*, "Growth of aligned multiwalled carbon nanotubes on bulk copper substrates by chemical vapor deposition," *Journal of Materials Research,* vol. 24, no. 9, pp. 2813-2820, Sep, 2009.

[27] S. Sotiropoulou, and N. A. Chaniotakis, "Carbon nanotube array-based biosensor," *Analytical and Bioanalytical Chemistry,* vol. 375, no. 1, pp. 103-105, Jan, 2003.

[28] H. Ago, N. Uehara, K. Ikeda *et al.*, "Synthesis of horizontally-aligned single-walled carbon nanotubes with controllable density on sapphire surface and polarized Raman spectroscopy," *Chemical Physics Letters,* vol. 421, no. 4-6, pp. 399-403, Apr 15, 2006.

[29] V. Derycke, R. Martel, M. Radosvljevic *et al.*, "Catalyst-free growth of ordered single-walled carbon nanotube networks," *Nano Letters,* vol. 2, no. 10, pp. 1043-1046, Oct, 2002.

[30] N. Saurakhiya, Y. W. Zhu, F. C. Cheong *et al.*, "Pulsed laser deposition-assisted patterning of aligned carbon nanotubes modified by focused laser beam for efficient field emission," *Carbon,* vol. 43, no. 10, pp. 2128-2133, Aug, 2005.

[31] J. S. Suh, K. S. Jeong, J. S. Lee *et al.*, "Study of the field-screening effect of highly ordered carbon nanotube arrays," *Applied Physics Letters,* vol. 80, no. 13, pp. 2392-2394, Apr 1, 2002.

[32] H. Ago, T. Komatsu, S. Ohshima *et al.*, "Dispersion of metal nanoparticles for aligned carbon nanotube arrays," *Applied Physics Letters,* vol. 77, no. 1, pp. 79-81, Jul 3, 2000.
[33] B. Q. Wei, R. Vajtai, Y. Jung *et al.*, "Organized assembly of carbon nanotubes - Cunning refinements help to customize the architecture of nanotube structures.," *Nature,* vol. 416, no. 6880, pp. 495-496, Apr 4, 2002.
[34] D. S. Xu, G. L. Guo, L. L. Gui *et al.*, "Controlling growth and field emission property of aligned carbon nanotubes on porous silicon substrates," *Applied Physics Letters,* vol. 75, no. 4, pp. 481-483, Jul 26, 1999.
[35] Y. Wang, K. Kempa, B. Kimball *et al.*, "Receiving and transmitting light-like radio waves: Antenna effect in arrays of aligned carbon nanotubes," *Applied Physics Letters,* vol. 85, no. 13, pp. 2607-2609, Sep 27, 2004.
[36] C. V. Nguyen, L. Delzeit, A. M. Cassell *et al.*, "Preparation of nucleic acid functionalized carbon nanotube Arrays," *Nano Letters,* vol. 2, no. 10, pp. 1079-1081, Oct, 2002.
[37] K. M. Ryu, A. Badmaev, L. Gomez *et al.*, "Synthesis of aligned single-walled nanotubes using catalysts defined by nanosphere lithography," *Journal of the American Chemical Society,* vol. 129, no. 33, pp. 10104-+, Aug 22, 2007.
[38] Z. W. Pan, S. S. Xie, B. H. Chang *et al.*, "Direct growth of aligned open carbon nanotubes by chemical vapor deposition," *Chemical Physics Letters,* vol. 299, no. 1, pp. 97-102, Jan 1, 1999.
[39] J. F. AuBuchon, C. Daraio, L. H. Chen *et al.*, "Iron silicide root formation in carbon nanotubes grown by microwave PECVD," *Journal of Physical Chemistry B,* vol. 109, no. 51, pp. 24215-24219, Dec 29, 2005.
[40] N. Hayashi, S. Honda, K. Tsuji *et al.*, "Highly aligned carbon nanotube arrays fabricated by bias sputtering," *Applied Surface Science,* vol. 212, pp. 393-396, May 15, 2003.
[41] H. F. Zhao, H. Song, Z. M. Li *et al.*, "Electrophoretic deposition and field emission properties of patterned carbon nanotubes," *Applied Surface Science,* vol. 251, no. 1-4, pp. 242-244, Sep 15, 2005.
[42] N. S. Lee, D. S. Chung, I. T. Han *et al.*, "Application of carbon nanotubes to field emission displays," *Diamond and Related Materials,* vol. 10, no. 2, pp. 265-270, Feb, 2001.
[43] Y. M. Shin, S. Y. Jeong, H. J. Jeong *et al.*, "Influence of morphology of catalyst thin film on vertically aligned carbon nanotube growth," *Journal of Crystal Growth,* vol. 271, no. 1-2, pp. 81-89, Oct 15, 2004.
[44] R. M. Liu, J. M. Ting, J. C. A. Huang *et al.*, "Growth of carbon nanotubes and nanowires using selected catalysts," *Thin Solid Films,* vol. 420, pp. 145-150, Dec 2, 2002.
[45] K. Kempa, B. Kimball, J. Rybczynski *et al.*, "Photonic crystals based on periodic arrays of aligned carbon nanotubes," *Nano Letters,* vol. 3, no. 1, pp. 13-18, Jan, 2003.
[46] Z. P. Huang, D. L. Carnahan, J. Rybczynski *et al.*, "Growth of large periodic arrays of carbon nanotubes," *Applied Physics Letters,* vol. 82, no. 3, pp. 460-462, Jan 20, 2003.

[47] E. Joselevich, and C. M. Lieber, "Vectorial growth of metallic and semiconducting single-wall carbon nanotubes," *Nano Letters,* vol. 2, no. 10, pp. 1137-1141, Oct, 2002.
[48] Y. G. Zhang, A. L. Chang, J. Cao *et al.*, "Electric-field-directed growth of aligned single-walled carbon nanotubes," *Applied Physics Letters,* vol. 79, no. 19, pp. 3155-3157, Nov 5, 2001.
[49] K. H. Lee, J. M. Cho, and W. Sigmund, "Control of growth orientation for carbon nanotubes," *Applied Physics Letters,* vol. 82, no. 3, pp. 448-450, Jan 20, 2003.
[50] N. Kumar, W. Curtis, and J. I. Hahm, "Laterally aligned, multiwalled carbon nanotube growth using Magnetospirillium magnetotacticum," *Applied Physics Letters,* vol. 86, no. 17, pp. -, Apr 25, 2005.
[51] S. M. Huang, X. Y. Cai, and J. Liu, "Growth of millimeter-long and horizontally aligned single-walled carbon nanotubes on flat substrates," *Journal of the American Chemical Society,* vol. 125, no. 19, pp. 5636-5637, May 14, 2003.
[52] S. M. Huang, B. Maynor, X. Y. Cai *et al.*, "Ultralong, well-aligned single-walled carbon nanotube architectures on surfaces," *Advanced Materials,* vol. 15, no. 19, pp. 1651-+, Oct 2, 2003.
[53] S. M. Huang, Q. Fu, L. An *et al.*, "Growth of aligned SWNT arrays from water-soluble molecular clusters for nanotube device fabrication," *Physical Chemistry Chemical Physics,* vol. 6, no. 6, pp. 1077-1079, Mar 21, 2004.
[54] D. Sanchez-Portal, E. Artacho, J. M. Soler *et al.*, "Ab initio structural, elastic, and vibrational properties of carbon nanotubes," *Physical Review B,* vol. 59, no. 19, pp. 12678-12688, May 15, 1999.
[55] M. M. J. Treacy, T. W. Ebbesen, and J. M. Gibson, "Exceptionally high Young's modulus observed for individual carbon nanotubes," *Nature,* vol. 381, no. 6584, pp. 678-680, Jun 20, 1996.
[56] E. W. Wong, P. E. Sheehan, and C. M. Lieber, "Nanobeam mechanics: Elasticity, strength, and toughness of nanorods and nanotubes," *Science,* vol. 277, no. 5334, pp. 1971-1975, Sep 26, 1997.
[57] G. H. Gao, T. Cagin, and W. A. Goddard, "Energetics, structure, mechanical and vibrational properties of single-walled carbon nanotubes," *Nanotechnology,* vol. 9, no. 3, pp. 184-191, Sep, 1998.
[58] E. Hernandez, C. Goze, P. Bernier *et al.*, "Elastic properties of C and BxCyNz composite nanotubes," *Physical Review Letters,* vol. 80, no. 20, pp. 4502-4505, May 18, 1998.
[59] M. F. Yu, B. S. Files, S. Arepalli *et al.*, "Tensile loading of ropes of single wall carbon nanotubes and their mechanical properties," *Physical Review Letters,* vol. 84, no. 24, pp. 5552-5555, Jun 12, 2000.
[60] H. W. Zhu, C. L. Xu, D. H. Wu *et al.*, "Direct synthesis of long single-walled carbon nanotube strands," *Science,* vol. 296, no. 5569, pp. 884-886, May 3, 2002.
[61] L. T. Qu, L. M. Dai, M. Stone *et al.*, "Carbon nanotube arrays with strong shear binding-on and easy normal lifting-off," *Science,* vol. 322, no. 5899, pp. 238-242, Oct 10, 2008.
[62] J. Hone, B. Batlogg, Z. Benes *et al.*, "Quantized phonon spectrum of single-wall carbon nanotubes," *Science,* vol. 289, no. 5485, pp. 1730-1733, Sep 8, 2000.

[63] W. Yi, L. Lu, D. L. Zhang *et al.*, "Linear specific heat of carbon nanotubes," *Physical Review B,* vol. 59, no. 14, pp. R9015-R9018, Apr 1, 1999.
[64] J. C. Lasjaunias, K. Biljakovic, Z. Benes *et al.*, "Low-temperature specific heat of single-wall carbon nanotubes," *Physical Review B,* vol. 65, no. 11, pp. -, Mar 15, 2002.
[65] V. N. Popov, "Low-temperature specific heat of nanotube systems," *Physical Review B,* vol. 66, no. 15, pp. -, Oct 15, 2002.
[66] P. Kim, L. Shi, A. Majumdar *et al.*, "Thermal transport measurements of individual multiwalled nanotubes," *Physical Review Letters,* vol. 8721, no. 21, pp. -, Nov 19, 2001.
[67] S. Berber, Y. K. Kwon, and D. Tomanek, "Unusually high thermal conductivity of carbon nanotubes," *Physical Review Letters,* vol. 84, no. 20, pp. 4613-4616, May 15, 2000.
[68] S. Shaikh, L. Li, K. Lafdi *et al.*, "Thermal conductivity of an aligned carbon nanotube array," *Carbon,* vol. 45, no. 13, pp. 2608-2613, Nov, 2007.
[69] H. Huang, C. H. Liu, Y. Wu *et al.*, "Aligned carbon nanotube composite films for thermal management," *Advanced Materials,* vol. 17, no. 13, pp. 1652-+, Jul 4, 2005.
[70] Y. Xu, Y. Zhang, E. Suhir *et al.*, "Thermal properties of carbon nanotube array used for integrated circuit cooling (vol 100, art no 074302, 2006)," *Journal of Applied Physics,* vol. 100, no. 12, pp. -, Dec 15, 2006.
[71] L. Langer, L. Stockman, J. P. Heremans *et al.*, "Electrical-Resistance of a Carbon Nanotube Bundle," *Journal of Materials Research,* vol. 9, no. 4, pp. 927-932, Apr, 1994.
[72] L. Langer, V. Bayot, E. Grivei *et al.*, "Quantum transport in a multiwalled carbon nanotube," *Physical Review Letters,* vol. 76, no. 3, pp. 479-482, Jan 15, 1996.
[73] M. Bockrath, D. H. Cobden, P. L. McEuen *et al.*, "Single-electron transport in ropes of carbon nanotubes," *Science,* vol. 275, no. 5308, pp. 1922-1925, Mar 28, 1997.
[74] J. W. Mintmire, B. I. Dunlap, and C. T. White, "Are Fullerene Tubules Metallic," *Physical Review Letters,* vol. 68, no. 5, pp. 631-634, Feb 3, 1992.
[75] S. J. Tans, M. H. Devoret, H. J. Dai *et al.*, "Individual single-wall carbon nanotubes as quantum wires," *Nature,* vol. 386, no. 6624, pp. 474-477, Apr 3, 1997.
[76] L. B. Zhu, J. W. Xu, Y. H. Xiu *et al.*, "Growth and electrical characterization of high-aspect-ratio carbon nanotube arrays," *Carbon,* vol. 44, no. 2, pp. 253-258, Feb, 2006.
[77] W. A. Deheer, A. Chatelain, and D. Ugarte, "A Carbon Nanotube Field-Emission Electron Source," *Science,* vol. 270, no. 5239, pp. 1179-1180, Nov 17, 1995.
[78] W. A. Deheer, W. S. Bacsa, A. Chatelain *et al.*, "Aligned Carbon Nanotube Films - Production and Optical and Electronic-Properties," *Science,* vol. 268, no. 5212, pp. 845-847, May 12, 1995.
[79] S. S. Fan, M. G. Chapline, N. R. Franklin *et al.*, "Self-oriented regular arrays of carbon nanotubes and their field emission properties," *Science,* vol. 283, no. 5401, pp. 512-514, Jan 22, 1999.

[80] Y. N. Zhang, W. Lei, X. B. Zhang *et al.*, "Calculation of the emission performance of the carbon nanotube array," *Applied Surface Science,* vol. 245, no. 1-4, pp. 400-406, May 30, 2005.

[81] K. S. Hazra, P. Rai, D. R. Mohapatra *et al.*, "Dramatic Enhancement of the Emission Current Density from Carbon Nanotube Based Nanosize Tips with Extremely Low Onset Fields," *Acs Nano,* vol. 3, no. 9, pp. 2617-2622, Sep, 2009.

[82] B. Zhao, D. N. Futaba, S. Yasuda *et al.*, "Exploring Advantages of Diverse Carbon Nanotube Forests With Tailored Structures Synthesized by Supergrowth from Engineered Catalysts," *Acs Nano,* vol. 3, no. 1, pp. 108-114, Jan, 2009.

[83] L. Nilsson, O. Groening, C. Emmenegger *et al.*, "Scanning field emission from patterned carbon nanotube films," *Applied Physics Letters,* vol. 76, no. 15, pp. 2071-2073, Apr 10, 2000.

[84] J. C. Charlier, M. Terrones, M. Baxendale *et al.*, "Enhanced electron field emission in B-doped carbon nanotubes," *Nano Letters,* vol. 2, no. 11, pp. 1191-1195, Nov, 2002.

[85] A. C. Dillon, K. M. Jones, T. A. Bekkedahl *et al.*, "Storage of hydrogen in single-walled carbon nanotubes," *Nature,* vol. 386, no. 6623, pp. 377-379, Mar 27, 1997.

[86] C. Liu, Y. Y. Fan, M. Liu *et al.*, "Hydrogen storage in single-walled carbon nanotubes at room temperature," *Science,* vol. 286, no. 5442, pp. 1127-1129, Nov 5, 1999.

[87] Y. Ye, C. C. Ahn, C. Witham *et al.*, "Hydrogen adsorption and cohesive energy of single-walled carbon nanotubes," *Applied Physics Letters,* vol. 74, no. 16, pp. 2307-2309, Apr 19, 1999.

[88] H. W. Zhu, A. Y. Cao, X. S. Li *et al.*, "Hydrogen adsorption in bundles of well-aligned carbon nano tubes at room temperature," *Applied Surface Science,* vol. 178, no. 1-4, pp. 50-55, Jul 2, 2001.

[89] Q. Y. Wang, and J. K. Johnson, "Optimization of carbon nanotube arrays for hydrogen adsorption," *Journal of Physical Chemistry B,* vol. 103, no. 23, pp. 4809-4813, Jun 10, 1999.

[90] A. Misra, J. Giri, and C. Daraio, "Hydrogen Evolution on Hydrophobic Aligned Carbon Nanotube Arrays," *Acs Nano,* vol. 3, no. 12, pp. 3903-3908, Dec, 2009.

[91] J. Kong, N. R. Franklin, C. W. Zhou *et al.*, "Nanotube molecular wires as chemical sensors," *Science,* vol. 287, no. 5453, pp. 622-625, Jan 28, 2000.

[92] Q. F. Pengfei, O. Vermesh, M. Grecu *et al.*, "Toward large arrays of multiplex functionalized carbon nanotube sensors for highly sensitive and selective molecular detection," *Nano Letters,* vol. 3, no. 3, pp. 347-351, Mar, 2003.

[93] J. C. Claussen, A. D. Franklin, A. ul Haque *et al.*, "Electrochemical Biosensor of Nanocube-Augmented Carbon Nanotube Networks," *Acs Nano,* vol. 3, no. 1, pp. 37-44, Jan, 2009.

[94] H. Cai, X. N. Cao, Y. Jiang *et al.*, "Carbon nanotube-enhanced electrochemical DNA biosensor for DNA hybridization detection," *Analytical and Bioanalytical Chemistry,* vol. 375, no. 2, pp. 287-293, Jan, 2003.

[95] R. J. Chen, S. Bangsaruntip, K. A. Drouvalakis *et al.*, "Noncovalent functionalization of carbon nanotubes for highly specific electronic biosensors," *Proceedings of the National Academy of Sciences of the United States of America,* vol. 100, no. 9, pp. 4984-4989, Apr 29, 2003.

[96] J. Zhao, A. Buldum, J. Han *et al.*, "First-principles study of Li-intercalated carbon nanotube ropes," *Physical Review Letters,* vol. 85, no. 8, pp. 1706-1709, Aug 21, 2000.

[97] G. L. Che, B. B. Lakshmi, E. R. Fisher *et al.*, "Carbon nanotubule membranes for electrochemical energy storage and production," *Nature,* vol. 393, no. 6683, pp. 346-349, May 28, 1998.

[98] M. Endo, Y. A. Kim, T. Hayashi *et al.*, "Vapor-grown carbon fibers (VGCFs) - Basic properties and their battery applications," *Carbon,* vol. 39, no. 9, pp. 1287-1297, 2001.

[99] G. T. Wu, C. S. Wang, X. B. Zhang *et al.*, "Lithium insertion into CuO/carbon nanotubes," *Journal of Power Sources,* vol. 75, no. 1, pp. 175-179, Sep 1, 1998.

[100] B. Gao, A. Kleinhammes, X. P. Tang *et al.*, "Electrochemical intercalation of single-walled carbon nanotubes with lithium," *Chemical Physics Letters,* vol. 307, no. 3-4, pp. 153-157, Jul 2, 1999.

[101] R. Z. Ma, J. Liang, B. Q. Wei *et al.*, "Study of electrochemical capacitors utilizing carbon nanotube electrodes," *Journal of Power Sources,* vol. 84, no. 1, pp. 126-129, Nov, 1999.

[102] K. H. An, W. S. Kim, Y. S. Park *et al.*, "Electrochemical properties of high-power supercapacitors using single-walled carbon nanotube electrodes," *Advanced Functional Materials,* vol. 11, no. 5, pp. 387-392, Oct, 2001.

[103] C. M. Niu, E. K. Sichel, R. Hoch *et al.*, "High power electrochemical capacitors based on carbon nanotube electrodes," *Applied Physics Letters,* vol. 70, no. 11, pp. 1480-1482, Mar 17, 1997.

[104] H. Ago, K. Petritsch, M. S. P. Shaffer *et al.*, "Composites of carbon nanotubes and conjugated polymers for photovoltaic devices," *Advanced Materials,* vol. 11, no. 15, pp. 1281, Oct 20, 1999.

[105] J. van de Lagemaat, T. M. Barnes, G. Rumbles *et al.*, "Organic solar cells with carbon nanotubes replacing In2O3 : Sn as the transparent electrode," *Applied Physics Letters,* vol. 88, no. 23, Jun 5, 2006.

# Figures

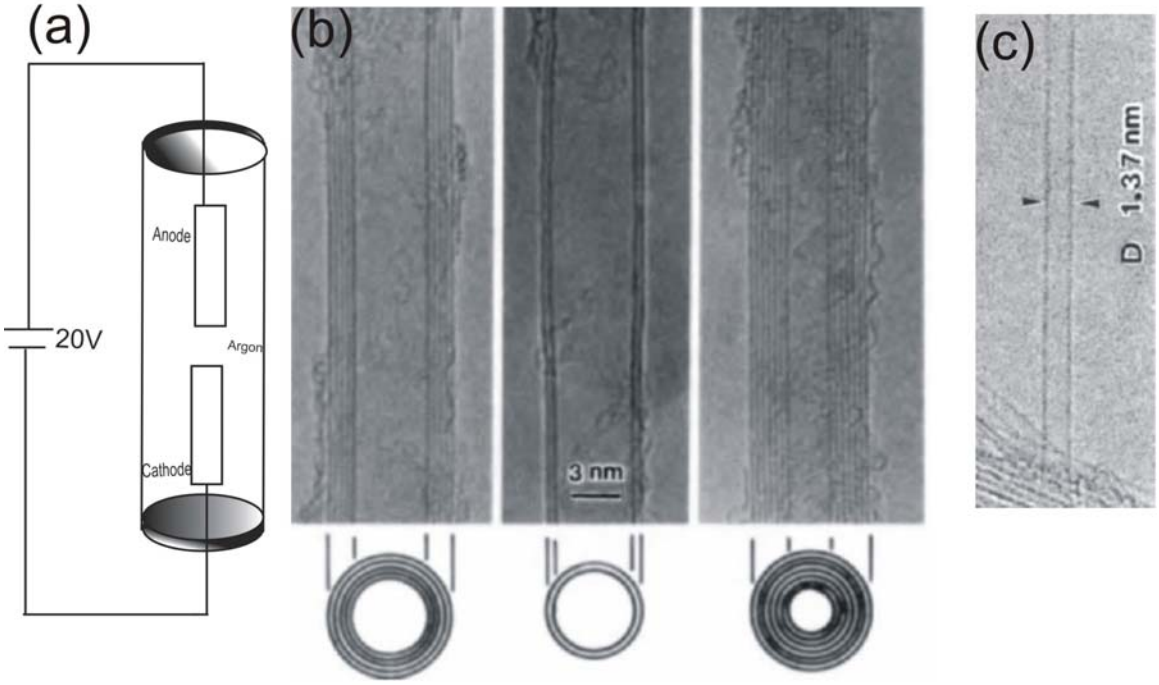


Figure 1: (a) Schematic of arc-discharge method. Two graphitic electrodes are typically 1 mm apart inside a quartz tube maintained at an argon pressure of 100 torr. An electric discharge is produced by passing high current of the order of 100 A at 20V. CNTs are collected at cathode. (b) Electron micrographs of CNTs having 5, 2 and 7 walls with diameter 6.7, 5.5 and 6.5 nm respectively. The CNT having seven layers have the smallest diameter [1]. (c) Electron micrograph of a SWNT showing the diameter of 1.37 nm produced by arc-discharge [2].

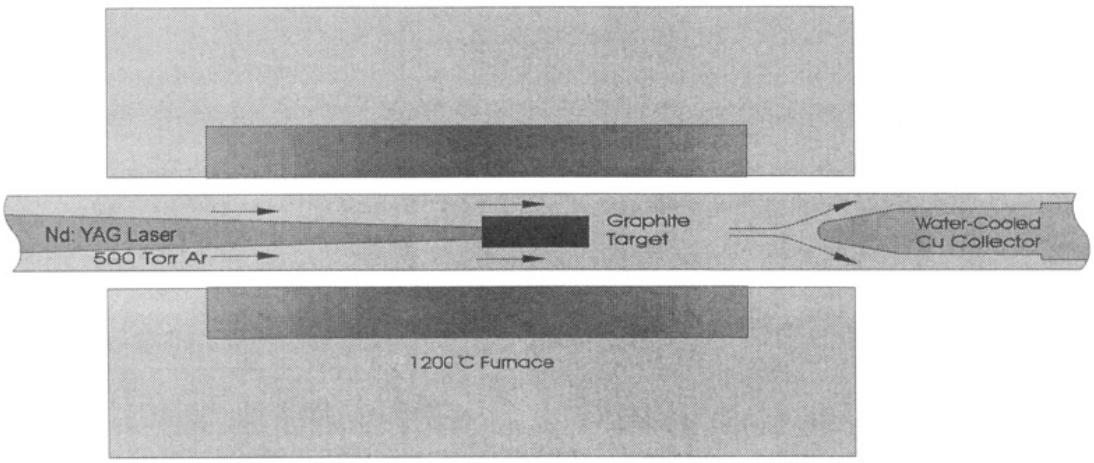


Figure 2: Schematic of the oven laser vaporization chamber for the growth of CNTs. MWNTs are synthesized using Nd:YAG laser pulses over a graphite target heated to 1200ºC inside a 50 cm long, 2.5 cm diameter quartz tube. The tube is maintained at the pressure of 500 torr by flowing Ar ata linear rate of 0.2 – 2 cm/s . Nanotubes are collected on the copper rod cooled by circulating water [4].

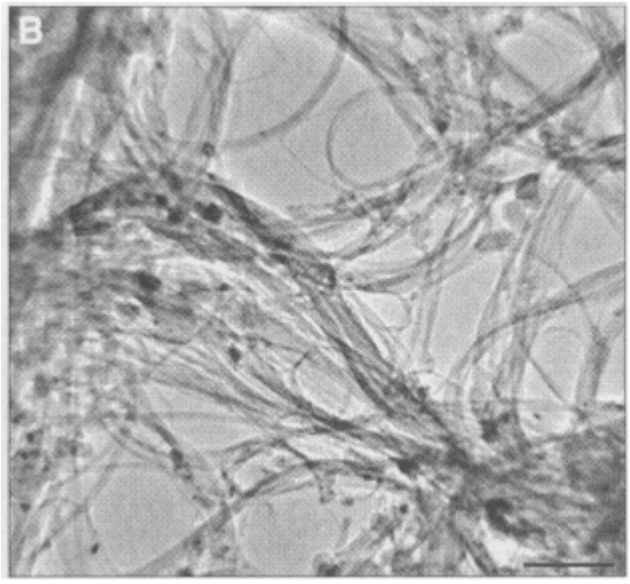


Figure 3: TEM image showing ropes of entangled SWNTs together with a small amount of catalyst particles coated with amorphous carbon. The scale bar is 100 nm [10].

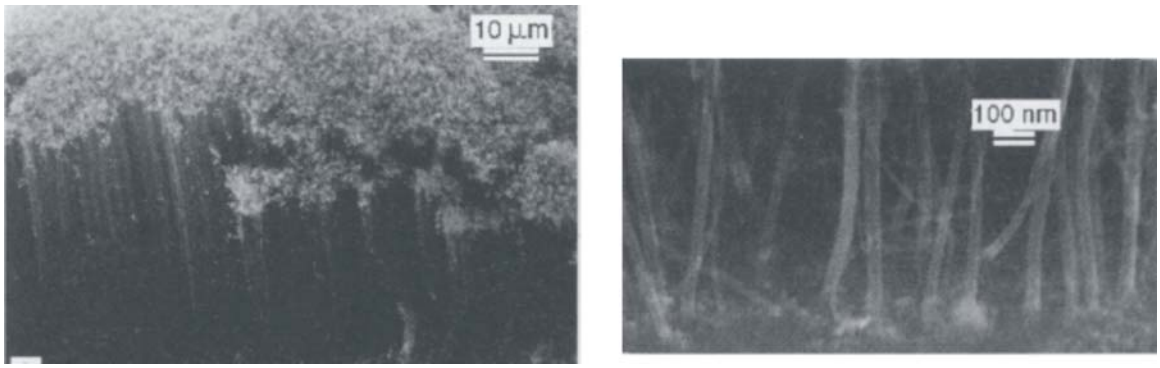


Figure 4: SEM images of vertically aligned CNTs. Left panel: Low magnification showing CNT film of thickness 50 μm Right panel: High magnification with CNTs of diameter ~ 30 nm and spacing ~ 100 nm [14].

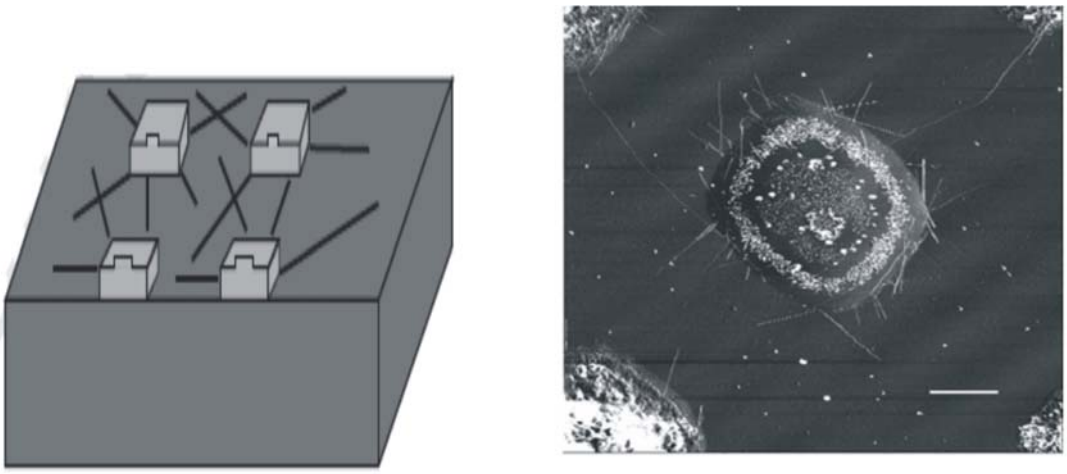

Figure 5: Left panel: Schematic of fabrication of catalytic island and CVD growth of aligned CNTs. Right panel: Large scale phase image recorded by tapping mode AFM showing CNTS grown from the patterned islands and bridging between islands. The scale bar is 2 μm [15]

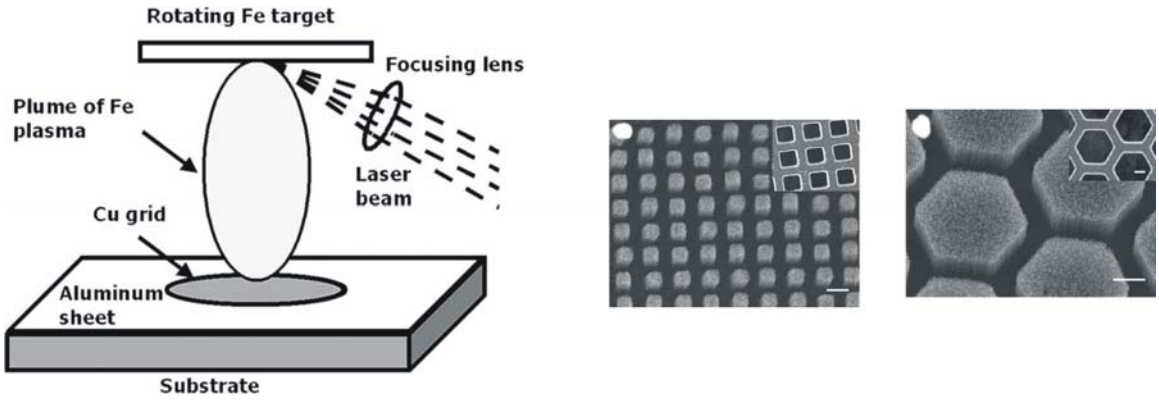


Figure 6: Left panel: Schematic of pulsed laser deposition to produce a thin film of Fe on Si substrate. The patterns are created using Cu grids used for TEM. Center panel: Rectangular array of CNTs grown by PECVD. Right panel: Hexagonal arrays of CNTs. The insets in the center and right figures show the square and hexagonal meshes used during the catalyst PLD deposition process. The scale bars are 10 μm [30].

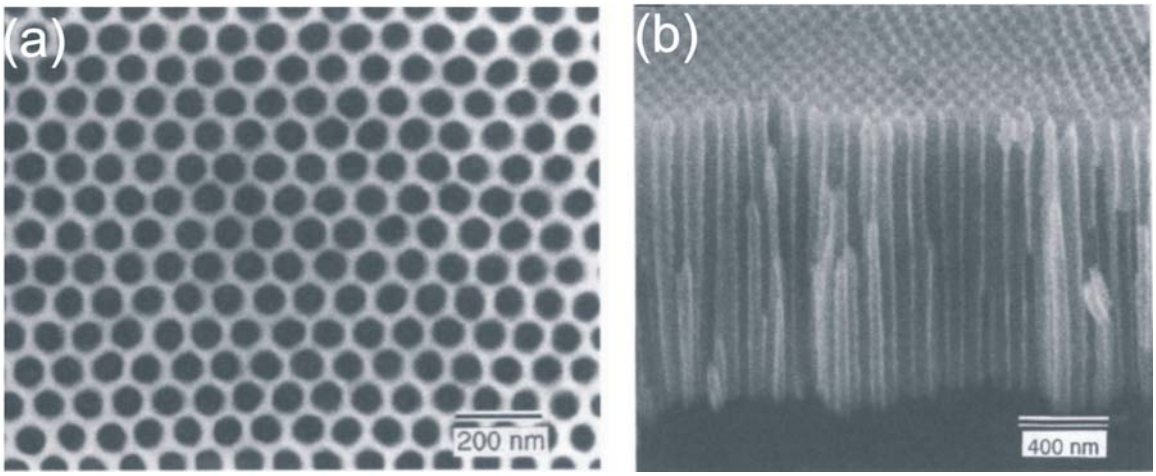


Figure 7: Typical SEM images of nanopore arrays (a) Top view (b) Cross-sectional view anodic aluminum oxide (**AAO**) **template** [21, 31].

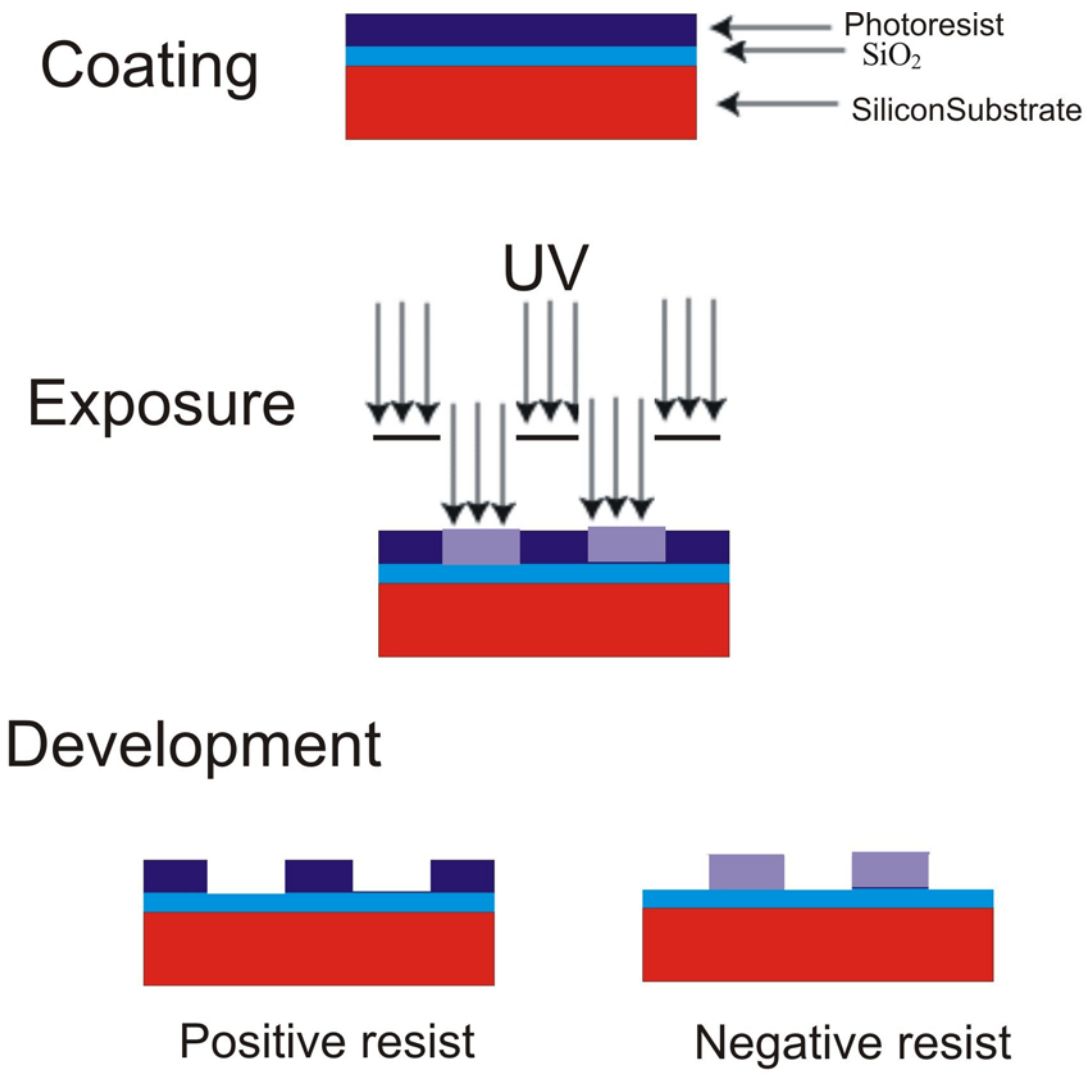


Figure 8: Schematic of the process of photolithography. A light sensitive material called photoresist is first coated on a silicon substrate. The spin-coating is followed by exposure to UV light through a mask. The exposed area of a positive resist materials dissolves in the developer solution while the unexposed region dissolves in the case of negative resist leaving behind the predetermined patterns of the mask.

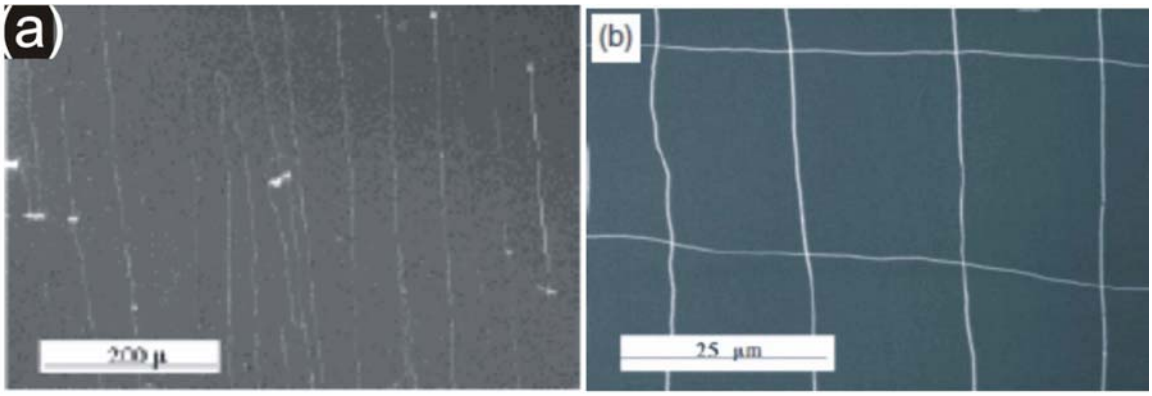


Figure 9: SEM images of (a) horizontally aligned SWNTs prepared by fast heating process and (b) networks formed by horizontal CNTs as a result of two step growth procedure [51]

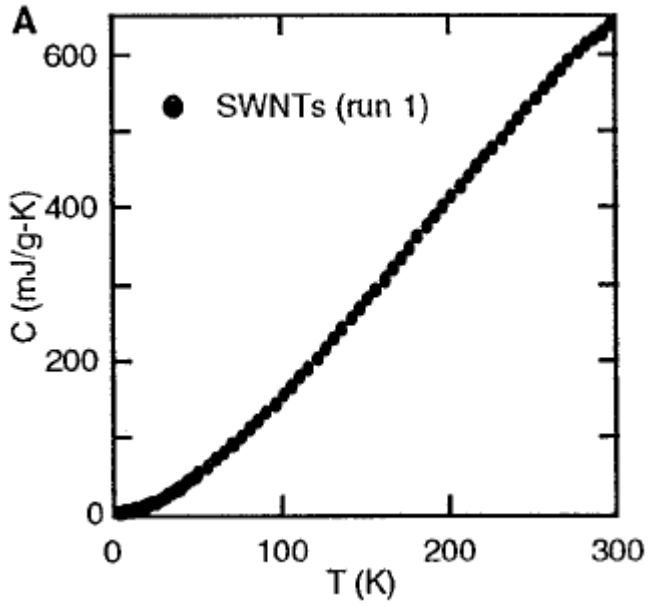


Figure 10: Specific heat of a sample consisting mainly of SWNT ropes on cooling from 300 – 2 K. The specific heat capacity of MWNTs exhibit linear dependence on temperature from 300 K to 1K while ~ $T^{0.62}$ dependence below 1 K [62].

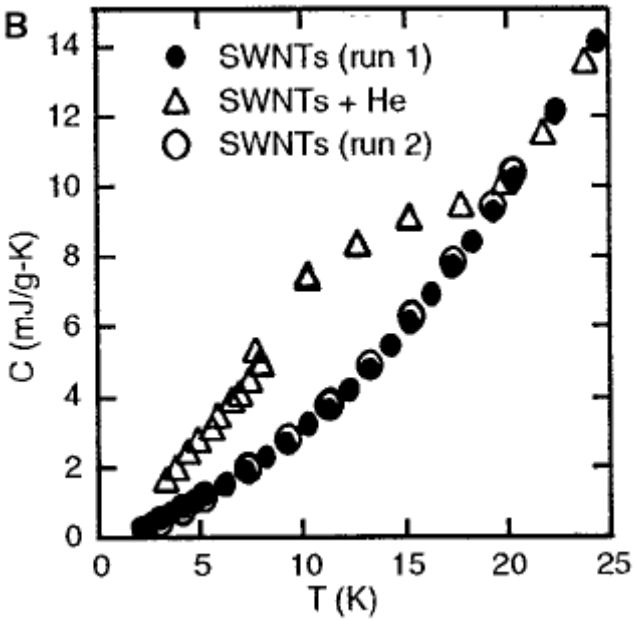


Figure 11: Low temperature behavior of specific heat: solid dots represent run 1, and open triangles represent a heating run after leaving the sample at 4 K overnight showing the effects of helium adsorption at 4 K and desorption at 20 K. Open circles were recorded for second cooling run after warming to 77 K and overlap perfectly with the first run. [62].

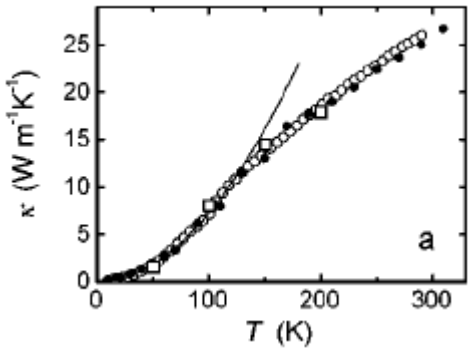


Figure 12: The temperate dependence of the thermal conductivity of MWNT samples. It is almost quadratic ($k \propto T^{1.98 \pm 0.03}$) at temperatures below 120 K and roughly linear above 120 K [63]

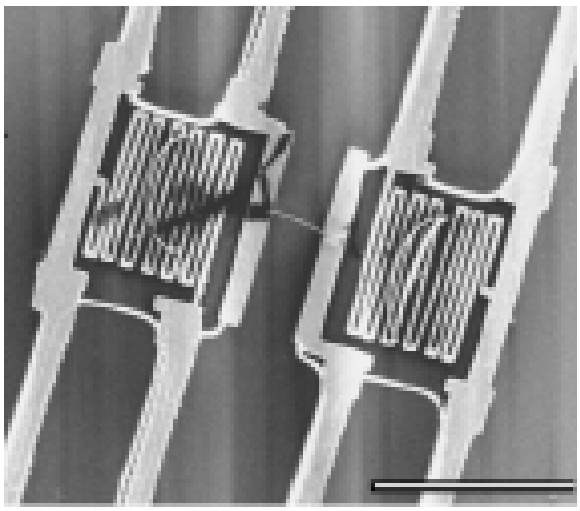

Figure 13: SEM image of a microfabricated device. The islands of two silicon nitride membranes are suspended on silicon nitride beams. A platinum thin film resistor serves as a heater on each of the islands. A small bundle of CNTs form a bridge between the islands to form a thermal contact. The scale bar is 10 μm [66].

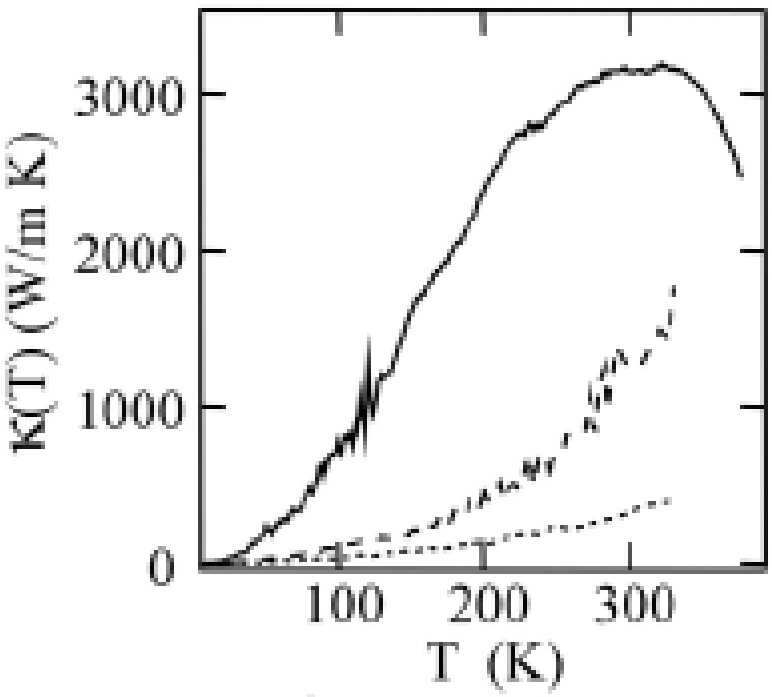


Figure 14: The temperate dependence of the thermal conductivity of MWNT samples [66]. It is almost quadratic ($k \propto T^{1.98 \pm 0.03}$) at temperatures below 120 K and roughly linear above 120 K [63]. Solid lines represent $\kappa(T)$ of an individual MWNT of diameter 14 nm. Broken and dotted lines are for bundles of diameters 80 nm and 200 nm.

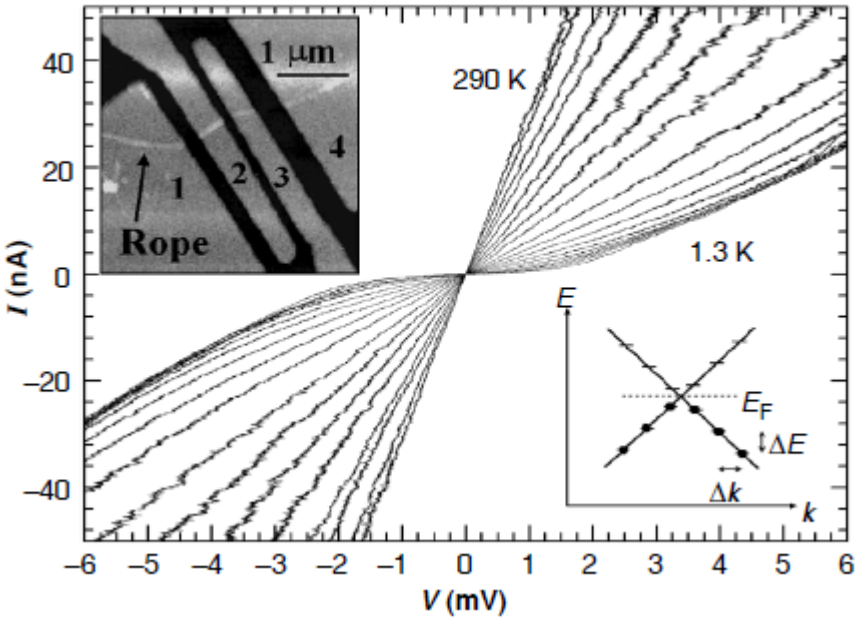


Figure 15: I-V characteristics at different temperatures for the rope segment between contacts 2 and 3. The left inset is an AFM image of the device fabricated to measure the electrical property of a CNT rope. Right inset is schematic energy-level diagram of the two 1D sub-bands near one of the Dirac points with *k* along the tube axis [73].

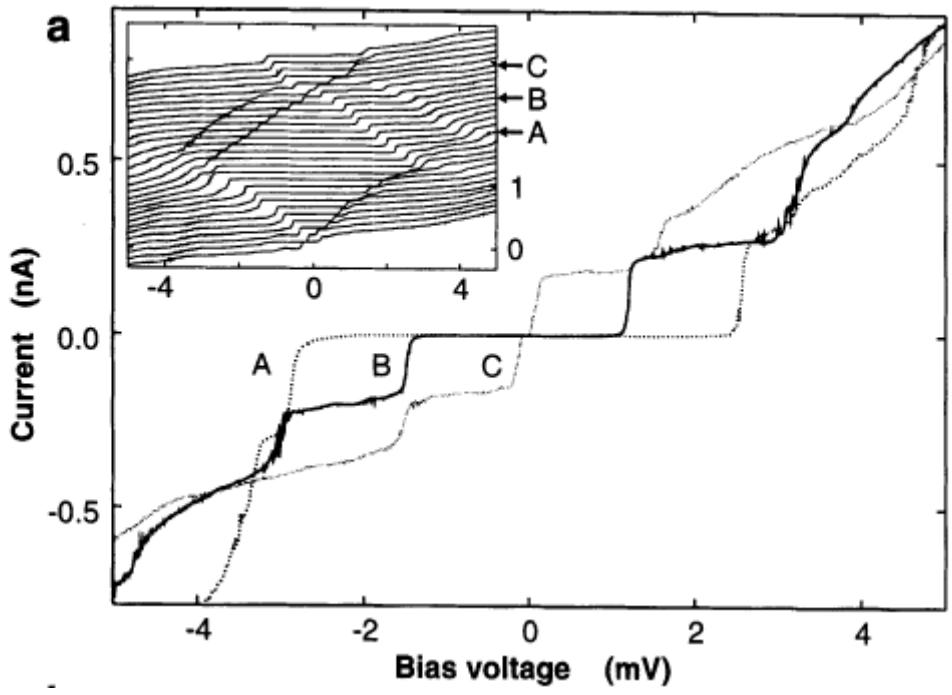


Figure 16: I-V characteristic of the nanotube at a gate voltage of 88.2 mV (trace A), 104.1 mV(trace B) and 120.0 mV (trace C). Inset shows more I-V curves with gate voltage ranging from 50mV (bottom) to 136 mV(top) [75].

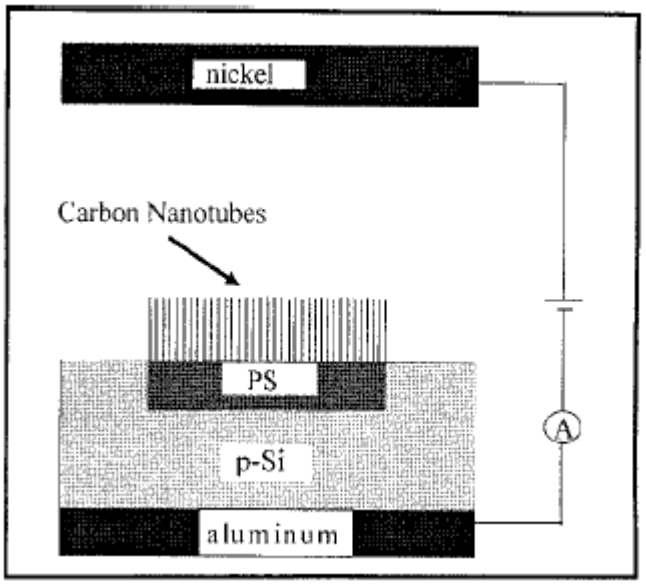


Figure 17: Experimental setup of measurement of field emission property. CNTs are used as cathodes [34]. A high electric field of the order of ~2V/μm is created between a metal anode and a CNT cathode to measure electron emission in low vacuum of ~$10^{-7}$ torr.

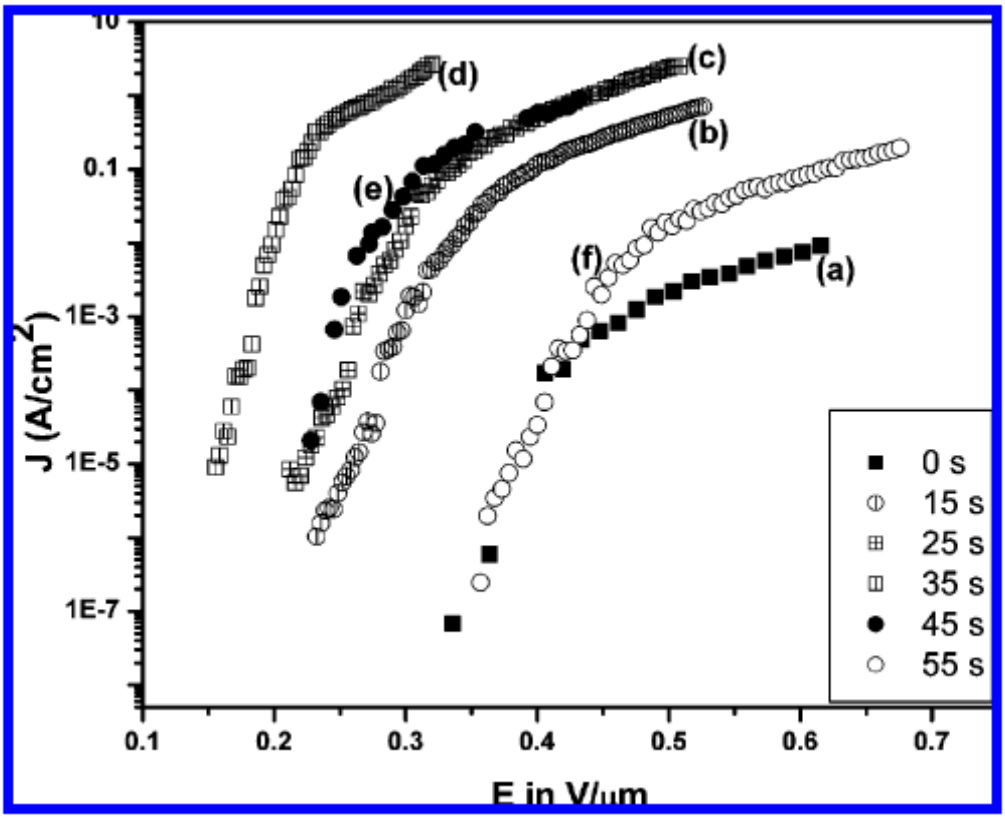


Figure 18: Typical field emission curves showing current density versus the electric field [81]. Emission current for CNTs with tips pruned for different times show different values at different electric fields. There is no electron emission below a threshold voltage.

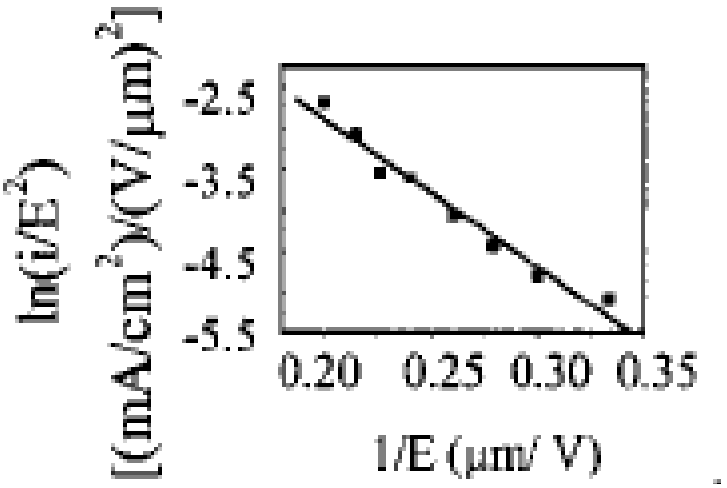


Figure 19: The straight line graph of logarithm of ($I/E^2$) versus 1/E, popularly called as Fowler-Nordheim (F-N) plot, is the evidence of field emission phenomenon [34].

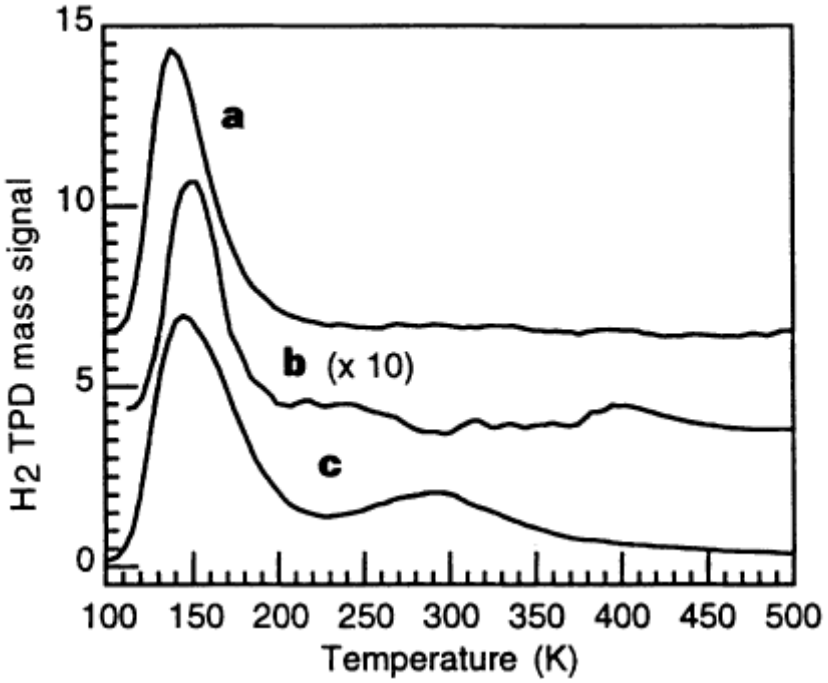


Figure 20: Temperature programmed desorption (TPD) spectra of hydrogen desorption [85]. a) TPD spectrum of as-produced SWNT sample after standard hydrogen exposure. b) TPD spectrum of activated carbon sample, magnified 10 times, after standard hydrogen exposure. c) TPD spectrum of SWNT sample after heating in vacuum to 970 K and standard hydrogen exposure.

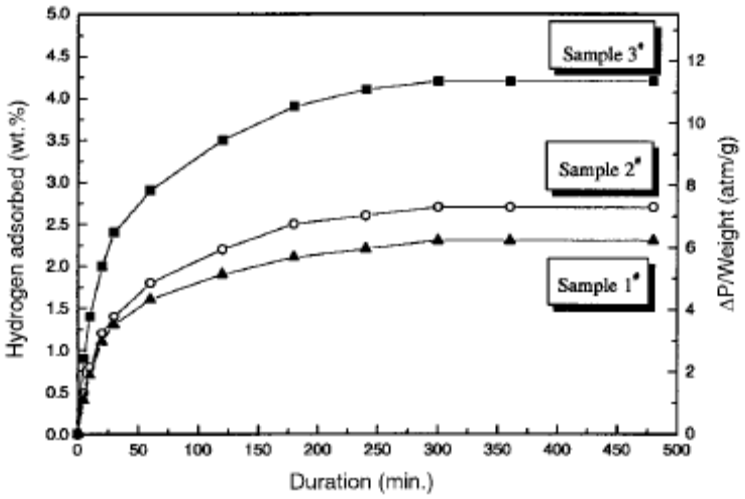


Figure 21: The Hydrogen uptake of SWNTs [86]. Sample 1 was used as-synthesized; Sample 2 was soaked in 37% HCl acid for 48 hrs, rinsed with deionized water and dried at 423K; Sample 3 was heated in a vacuum at 773K for two hrs after receiving the same treatment as sample 2. The heat treated SWNTs exhibited maximum hydrogen storage capacity of 4.2 wt % at the pressure of 10 MPa.

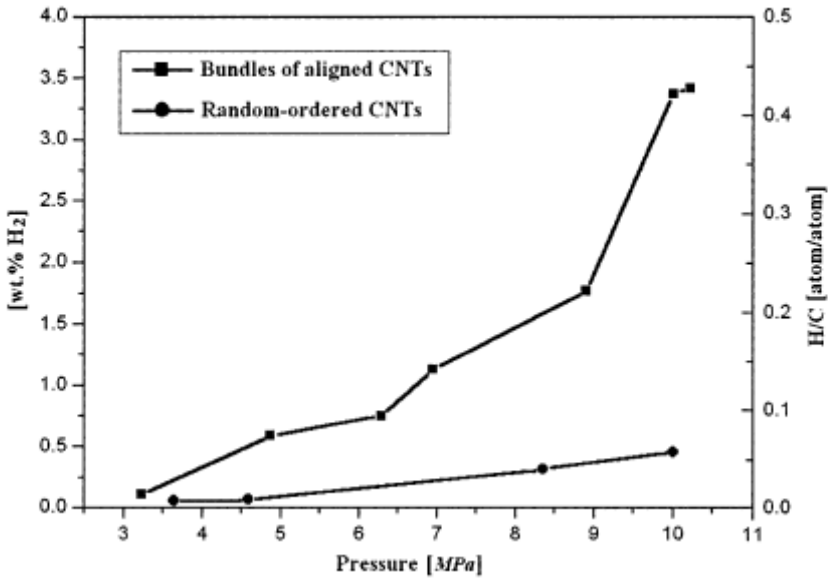


Figure 22: Comparison of $H_2$ adsorption between bundles of aligned SWNTs and random oriented SWNTs [88]. At lower pressures ~ 3.5 MPa, there is no significant difference in hydrogen adsorption between the aligned SWNTs and random SWNTs. However, aligned SWNTs exhibit a enhanced hydrogen storage at pressures ~ 10 MPa.

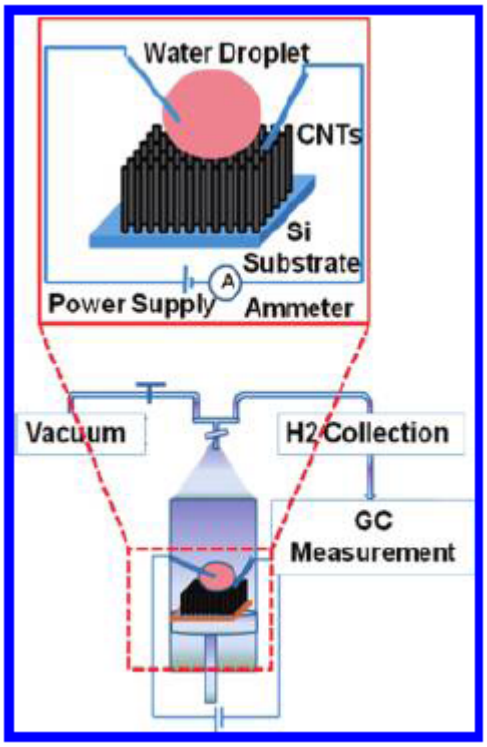


Figure 23: Schematic diagram of the experimental setup used for measuring the electrolytic reaction measurements on the CNT forests. The top section is the enlarged view for clarity of the sample area with the details on the probe's positioning [90].

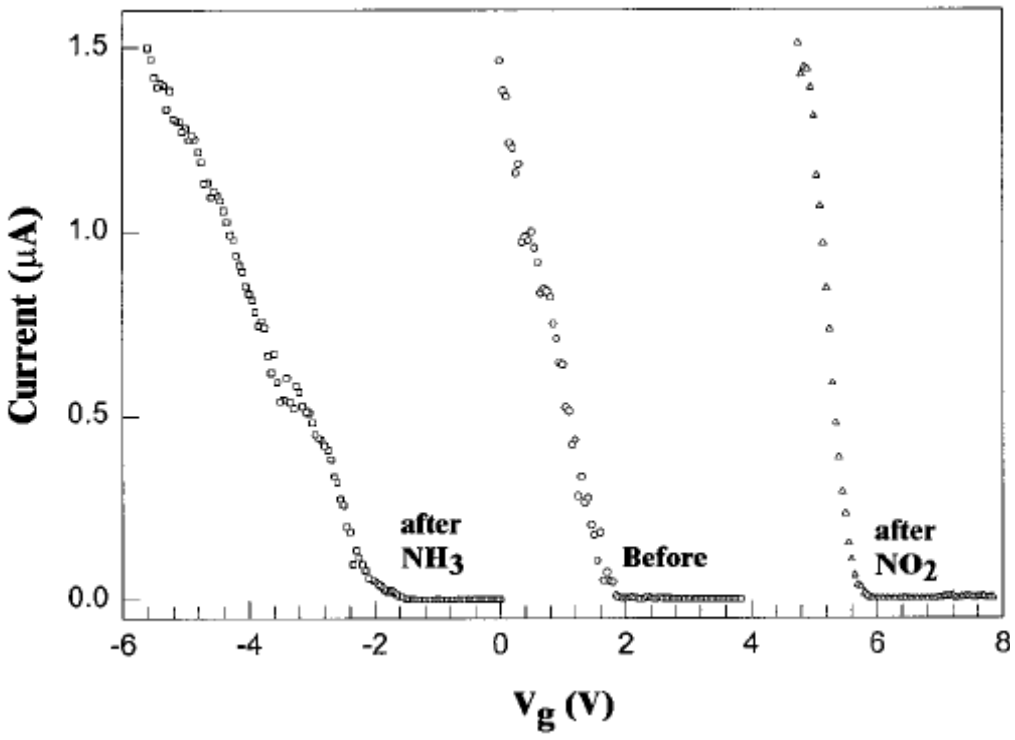


Figure 24: Current versus gate voltages curve before $NO_2$ (circles), after $NO_2$ (triangles) and after $NH_3$ (squares) [91]. There is an evident shift to the left in the I-$V_g$ curve by -4 V and shift towards right by + 4 V with the introduction of $NH_3$ and $NO_2$, respectively.

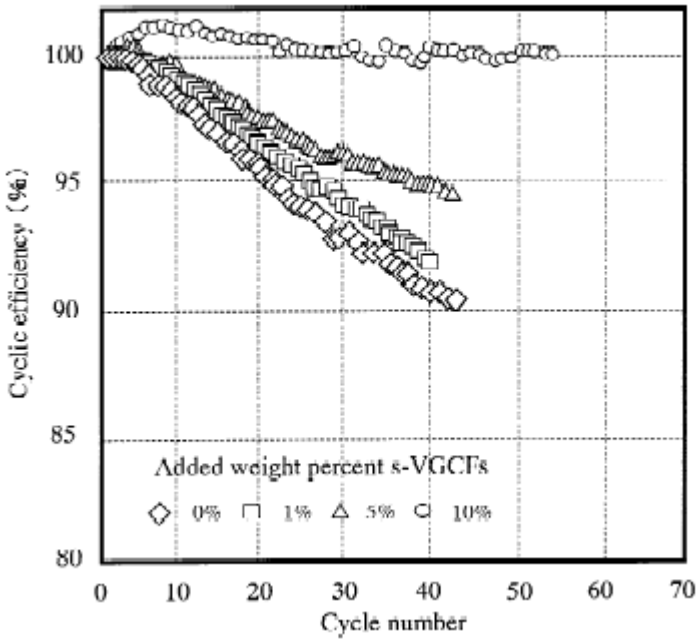


Figure 25: The cyclic efficiency of graphite as a function of added weight percent of CNTs [98]. The efficiency of graphitic anodes increased continuously until the composition of 10 wt % CNTs resulted in an efficiency of almost 100% up to 50 cycles

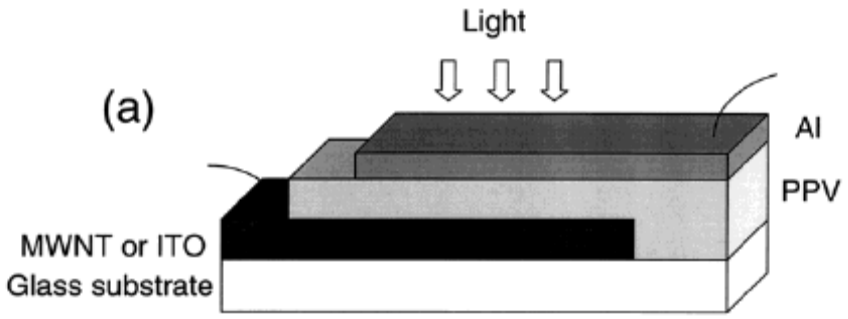


Figure 26: Schematic of a photovoltaic device. Visible light is shone through semi-transparent Al electrode and made to pass through polyphenylene vinylene ( PPV ) of thickness 210 nm and MWNT film of 140nm [104].

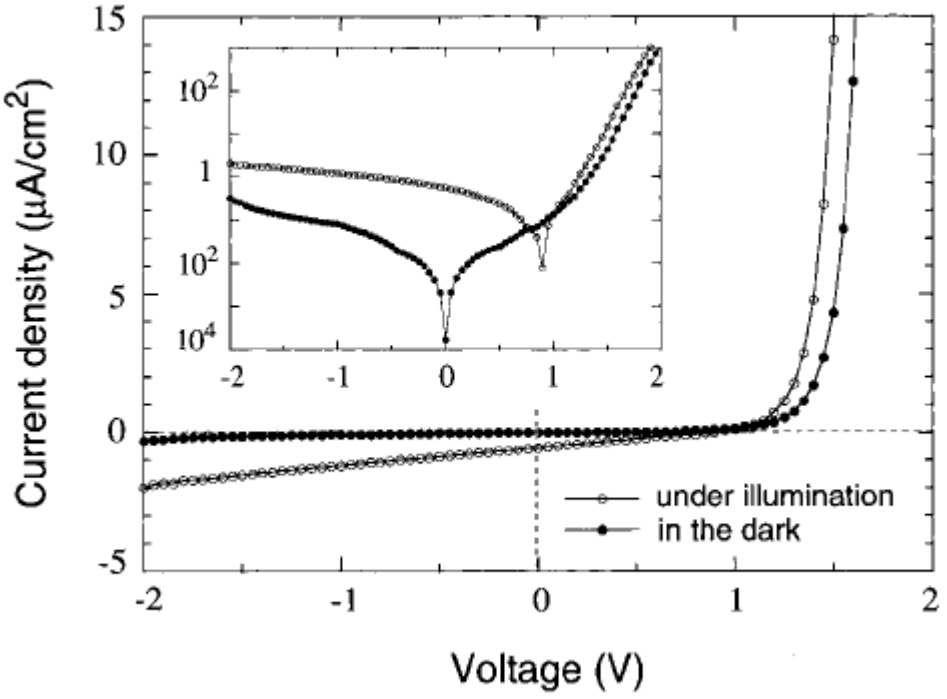


Figure 27: I-V characteristics of an MWNT/PPV/Al device in the dark (closed circles) and under illumination at a wavelength of 485 nm and intensity of 37μW/cm$^2$ (open circles). Inset is the representation of the same data with a logarithmic current axis [104].